Macromolecular Bioscience
www.mbs-journal.de

Recent Advances in 3D Printing of Photocurable Polymers: Types, Mechanism, and Tissue Engineering Application

*Aayushi Randhawa, Sayan Deb Dutta, Keya Ganguly, Dinesh K. Patel, Tejal V. Patil, and Ki-Taek Lim**

The conversion of liquid resin into solid structures upon exposure to light of a specific wavelength is known as photopolymerization. In recent years, photopolymerization-based 3D printing has gained enormous attention for constructing complex tissue-specific constructs. Due to the economic and environmental benefits of the biopolymers employed, photo-curable 3D printing is considered an alternative method for replacing damaged tissues. However, the lack of suitable bio-based photopolymers, their characterization, effective crosslinking strategies, and optimal printing conditions are hindering the extensive application of 3D printed materials in the global market. This review highlights the present status of various photopolymers, their synthesis, and their optimization parameters for biomedical applications. Moreover, a glimpse of various photopolymerization techniques currently employed for 3D printing is also discussed. Furthermore, various naturally derived nanomaterials reinforced polymerization and their influence on printability and shape fidelity are also reviewed. Finally, the ultimate use of those photopolymerized hydrogel scaffolds in tissue engineering is also discussed. Taken together, it is believed that photopolymerized 3D printing has a great future, whereas conventional 3D printing requires considerable sophistication, and this review can provide readers with a comprehensive approach to developing light-mediated 3D printing for tissue-engineering applications.

1. Introduction

Additive manufacturing, sometimes called rapid prototyping or 3D printing, was developed to create previously unachievable geometric forms and functions from well-defined materials used for traditional processing techniques like injection/blow molding and extrusion.[1] Additive manufacturing resulted in novel structural geometries made up of existing materials, whereas biology profited from developing processing techniques capable of accurately replicating nano-/microscale geometries. As a result, new medication delivery devices and tissue scaffolds have been developed.[2] For example, computer-aided design (CAD)/computer-aided manufacturing (CAM) procedures provide an automated means to generate a 3D shape of a chosen tissue structure and preciously controlled technology for future clinical applications of 3D bioprinting. Computed tomography and magnetic resonance imaging are medical imaging techniques that scan the patient to generate 3D volumetric information about the target object. The data from these imaging technologies are saved in the Digital Imaging and Communications in Medicine format, a standard digital imaging format, then reverse engineering methods to convert this data into a 3D CAD model. This technique starts with interpolating points inside and between picture slices to improve resolution and voxels from the measured data. To develop a surface model, localized volumetric data are extracted from a particular tissue structure, and a detailed reconstruction of the CAD model is necessary for the bioprinting process at this step. A CAM system generates a motion program, including instructions followed by proper structure slicing. The layer-by-layer procedure requires information from an object's sliced 2D forms. After that, tool path creation creates a path for the tool to follow to fill each layer's cross-sectional space. The printed tissue-specific architecture contains the inner functional structure of various cellular components for successful tissue regeneration. As a result, a well-organized tool path generation method is essential.

Photopolymerization-based 3D-printing techniques have piqued the interest of polymer chemists, material scientists, and engineers alike due to their versatility in polymer chemistry-related advances.[3,4] Photopolymerization is a method of forming a linear or crosslinked polymer structure by initiating and propagating a polymerization reaction using light.[5] Photopolymerization has recently been presented as a method for fabricating biomaterial-based polymer networks that can be customized for specialized biological applications. Furthermore, combining features held by photopolymerizable

A. Randhawa, S. D. Dutta, K. Ganguly, D. K. Patel, T. V. Patil, K.-T. Lim
Department of Biosystems Engineering
Kangwon National University
Chuncheon 24341, Republic of Korea
E-mail: ktlim@kangwon.ac.kr
A. Randhawa, T. V. Patil, K.-T. Lim
Interdisciplinary Program in Smart Agriculture
Kangwon National University
Chuncheon 24341, Republic of Korea

The ORCID identification number(s) for the author(s) of this article can be found under https://doi.org/10.1002/mabi.202200278

DOI: 10.1002/mabi.202200278

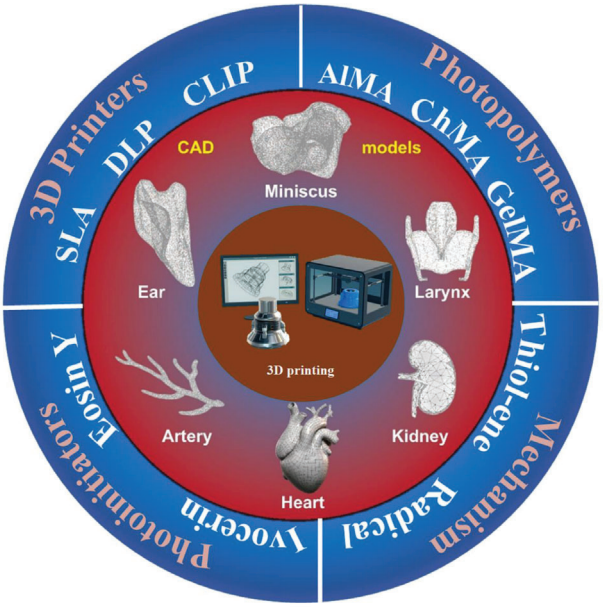

Figure 1. A schematic overview of the 3D printing of photocurable polymers and their design strategies based on the 3D CAD model. Printing techniques, such as stereolithography (SLA), digital light processing (DLP), and continuous liquid interface production (CLIP), employ UV and visible-light photoinitiators to initiate photopolymerization of polymers such as gelatin-methacrylate and chitosan-methacrylate in order to fabricate tissue-specific structures.

precursors and photopolymerized polymer networks has piqued interest beyond these applications. The following are essential characteristics for photopolymerized polymer development:[1] rapid synthesis and[2] the ability to transport in vivo or ex vivo photopolymerization. As a result, scientists have proposed that photopolymerized polymer networks be used in drug delivery,[6–8] tissue engineering, cell encapsulation, and as tissue barriers, fillers, biomimetic coatings and materials, adsorption membranes, contact lenses, and dental restorative materials, as well as for the fabrication of microfluidic devices, nanodevices, and nanopatterned surfaces.[9–11] When subjected to a specific wavelength of light, 3D photopolymerization (also referred to as photocuring or photo-crosslinking) can cure/photopolymerize monomers/oligomers in a liquid state to generate thermosets.[12] However, we must note that a photoinitiator or photoinitiator system with a relatively high absorption coefficient is required to transform photolytic energy into reactive species (radical or cation) that can drive chain formation via radical or cationic mechanisms.[13]

This paper emphasized the (bio)printing of different tissue constructs using synthetic and natural polymers, 3D printers, and their working mechanism. Moreover, the biomedical applications of the 3D printed structures are discussed. A schematic overview of this manuscript has been depicted in **Figure 1** to illustrate printing technologies and applications to the readers.

2. Photopolymerization in 3D Printing

Photopolymerization is typical for creating novel structures incorporated into the human body.[14] This is because this method allows us specific control not only on the geometry but also on the porosity contributed to the formulation of complex biological structures. This imbues the resultant fabricated structures to support cell survival and proliferation.[15] Furthermore, new bioprinting breakthroughs allow cell encapsulation in polymers for simultaneous deposition onto complex tissue scaffolds.[16] In contrast to conventional 3D printing methods, which use materials including ceramics, metal alloy, and thermoplastics, photopolymers are frequently used as inks for scaffold construction in photo-curable-based 3D-printing methods.[17] A promising approach to complicated tissue creation has been elucidated by combining polymers with biologically suitable hydrogel scaffolds. Tissue engineering entails the in vitro replication of native biological tissues for various purposes, including drug development, disease characterization, and organ replacement. Tissue scaffolds developed through nonspecific molding or finely adjusted 3D structures resemble the cell or organ of choice.[15] Tissue engineering incorporates synthetic and natural polymers, giving it various applications (refers to Tables S1 and S2, Supporting Information).

Photopolymerized 3D printing is divided into three categories:[1] stereolithography (SLA),[2] digital light processing (DLP), and[3] continuous liquid interface production (CLIP). All of these methods require a liquid as a starting material. Subsequently, light is utilized to harden the desired object, initiating the polymerization reaction in the process.[18] SLA involves photocrosslinking thin consecutive layers with UV or visible light to produce photopolymerization of a reactive system based on a sliced CAD model. Reactive or nonreactive diluents are commonly utilized, as the procedure requires a liquid photocrosslinkable resin with specific viscosity parameters. SLA can produce a large number of significantly varying 3D structures in a repeatable manner while maintaining the fine control over the final microstructure and shape.[19] On the other hand, DLP employs a digital micromirror device (DMD) to project a light mask that cures an entire layer in seconds via a mask projection-based procedure.[18] It cures a polymer resin layer in a single step, making it a rapid task.

3. Photocurable 3D Printing Technology: Type of 3D Printing Techniques

3D printing is a method of constructing 3D structures by layering materials (such as polymers) on top of each other. The photochemical approach is particularly appealing among the many 3D-printing approaches because objects may be generated using the photopolymerization processes of monomers/oligomers, which have environmental, economical, and industrial advantages.[4] In this approach, photoinitiators and monomers/oligomers are two of the most significant photopolymer components for 3D printing. Photoinitiators absorb a 3D printer's irradiation light and activate layer-by-layer photopolymerization processes of monomers/oligomers to form the specified 3D objects, while monomers/oligomers can define the printer's final characteristics printed product.[4] Composite materials and ceramic (Al_2O_3, ZrO_2, etc.) objects are increasingly fabricated using these lithographic 3D printing techniques. However, adding nano- and microscale fillers to photo-resins can cause increased resin viscosity,

inhomogeneity caused by settling filler particles, and light scattering. Standard triangulation language (STL) particularly specifies the surface of a 3D model as a network of triangles of varying sizes, depending on the desired resolution. The smaller the triangles, the more accurately the triangular mesh replicates the intended surface, resulting in a smoother to-be-printed product surface. Preprocessing refers to the stage in which the desired mesh model is created. Therefore, the choice of suitable crosslinker, polymer/prepolymer composition, and resin chemistry is crucial for the 3D printing of large-scale constructs.

Processing is the second stage of production. Because a 3D-printed object is built layer-by-layer, each subsequent layer must be supported by the platform, the layer before it, or additional support features. The STL model, including the supports, is cut into layers parallel to the platform surface, namely, the x–y plane, after creating the correct and optimal orientation of the model and the supports. The layers are created in the Oz direction, one after the other. The thickness of the layers is determined by the printer, additive manufacturing (AM) technology, and quality standards. After that, the sliced model is transmitted to the printer. Unlike traditional subtractive manufacturing (machining), which removes material from a workpiece, AM allows for more efficient material usage. In a stage known as post-processing, the model is removed from the platform after printing is completed, and various technological processing methods are performed to refine the printed product. The as-built models are rinsed in a wash solution, most frequently isopropyl alcohol, to remove the liquid coating of resin in the case of photopolymerization. These models are then artificially cured with UV radiation or exposed to sunlight naturally to improve their mechanical characteristics. Support removal, grinding, sealing, gluing, polishing, painting, varnishing, coating, sterilizing, inspection, and measuring are other procedures. Photopolymer parts require special post-processing. It is worth noting that the washing time, temperature, and curing time all define the mechanical qualities of final products.

3.1. Stereolithography (SLA)-Based Printing

The photopolymerization theory ultimately underpins SLA. The photo-initiator produces free radicals when interacting with UV light.[20] Localized polymerization occurs when the photosensitive liquid resin is exposed to the UV laser **Figure 2**a. UV light can move perpendicular to the liquefied resin surface in SLA. When a deposit has been set after exposure, another liquid resin layer is applied. This process is repeated until the end product is complete. When a product is finished, an excess amount of resin is pumped out and saved for future use. The finished object is cleaned to remove any excess resin. The support assemblies are then detachable. In general, like the casted parts, the printed portion has a few rough appearances that are improved with the coating.[21] Laser-based manufacturing is in high demand for a variety of reasons, including a) high-resolution part manufacturing, b) better surface finish without the need for post-processing, c) improved z-axis growth due to optimal bonding among the printed layers, and d) shorter time requirements than traditional methods. The cured layer thickness, dependent on the light energy given, is an essential parameter in SLA printing. Laser-based stereolithography has been widely used in dentistry and cardiac tissue engineering (Figure 2c) to build precise structures and biomedical devices.[22]

Coherent light sources (typically UV-emitting lasers) are employed in SLA systems to induce polymerization and crosslinking of the initial liquid resin. The high spatial resolution afforded by the focused laser beam's spot size is one of the critical advantages of SLA. Light exposure is conducted sequentially with SLA by scanning the laser beam within the plane on the surface of the photosensitive material. The amount of time it takes to make one slice of the structure is determined by the speed with which the laser beam is scanned and the size of the lighted area. A pair of mirrors within a Galvano-scanner is typically used to adjust the laser beam's lateral location. The procedure is carried out just like most other AM methods. The slice data are supplied as coordinates defining the two mirrors' tilt angle that guides the laser beam's position along the plane. Because each layer's pixel is irradiated sequentially, the exposure dose for each pixel could theoretically be adjusted separately by adjusting the laser intensity. SLA can now process grayscale patterns. The light penetration depth, which may be regulated by adding good absorbers to the photopolymer resin, determines vertical resolution. The exposure dose (light intensity and illumination time) affects the curing depth, which may be why SLA's grayscale capability is rarely used in practice. It is worth mentioning that the deposition of a new layer of photosensitive material, not laser scanning, is the most time-consuming process in SLA. The viscosity of the substance is crucial in this case. Nonreactive additives or solvents are frequently utilized to reduce the viscosity of the photopolymer resin. Micro-stereolithography (m-SLA) is a variation of standard SLA that is impractically slow for large structures but has a lateral resolution of a few micrometers.[28] The SLA technology is emerging and can be utilized to generate an advanced carrier for enzyme immobilization which partially satisfies the requirements of industrial enzyme catalysis synthesis.[29]

3.2. Digital Light Processing (DLP)-Based Printing

DLP-based 3D-printing technologies have recently marked a paradigm shift in traditional 3D-printing modalities, mainly by substantially boosting manufacturing rates and resolution. Rather than operating in serial ways like traditional inkjet and extrusion printers, a complete plane of the object is created at once. A light source, usually UV (365 nm) or visible light (410 nm), illuminates a DMD chip configured to project various digital patterns through a set of optics into a photopolymerizable vat, as well as a motorized build platform to control the height of the build. Because each micromirror on the DMD chip represents one pixel in the digital image, microscale feature sizes as tiny as 3–5 μm can be reached with suitable optics. As a result, highly complex biomimetic structures with medically realistic topological feature sizes can be quickly created. In DLP printing, the resin solution used to create 3D objects does not require precise adjusting for physicochemical qualities, including viscosity and surface tension.[30]

Fabrication of luminous 3D structures, extremely stretchy photopolymers, designed nerve guiding conduits, re-processable

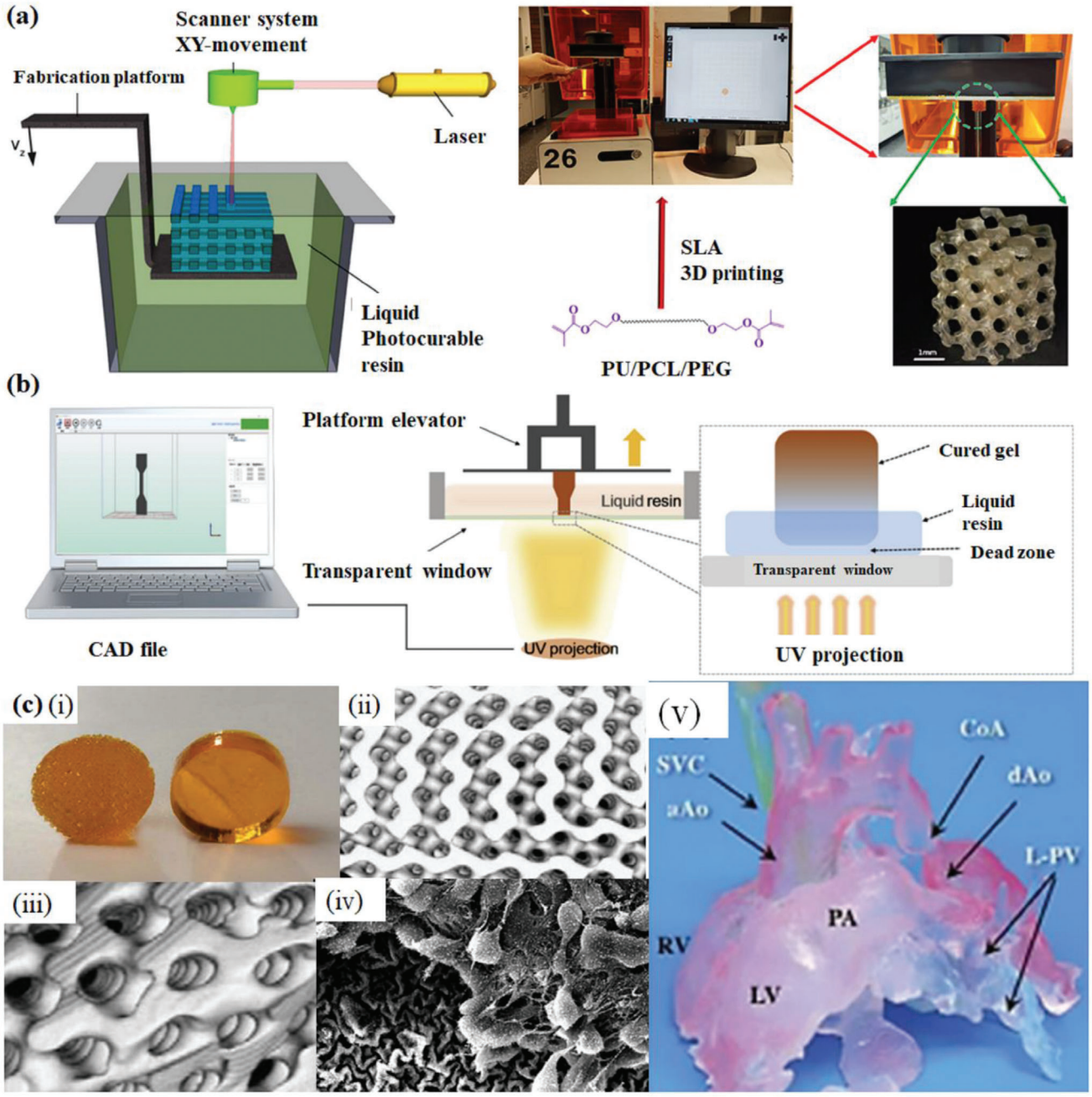

Figure 2. Schematic images of different laser-based hydrogel 3D printing systems. a) Stereolithography apparatus. Reproduced with permission.[23] Copyright 2012, Elsevier, and SLA manufacturing setup for a 3D printed scaffold made from photocurable PU/PCL/PEG resin. Reproduced with permission.[24] Copyright 2020, Elsevier. b) A typical CLIP printer's functioning mechanism is shown schematically. Reproduced with permission.[25] Copyright 2020, Elsevier. c) i) SLA-printed PDLLA-PEG-PDLLA hydrogel; ii, iii) μCT (microcomputed tomography imaging) analysis of the designed hydrogel; iv) SEM image of the cells attached to porous hydrogel scaffold. Reproduced with permission.[26] Copyright 2010, Elsevier. v) A bio model of a 2 month old heart with isolated aortic coarctation was printed using SLA technology. Reproduced with permission.[27] Copyright 2010, Elsevier.

thermosets, electrically conductive constructs, organic–inorganic hybrid networks, and other complicated objects have all been done with DLP-based printing. Patient personalized medical equipment with a precision of 40 × 40 μm can be created using DLP-based printers (at 465 nm), which are helpful for smooth-surfaced medical devices or bone scaffolds.

DLP and SLA use light to crosslink photo-resins layer-by-layer to create a free-standing object selectively. Unlike SLA, each layer is exposed all at once using a selectively veiled light source rather than one by one. DLP is called dynamic mask photolithography since it closely mimics traditional lithography. Black and white photos offer information for each layer of the structure. A

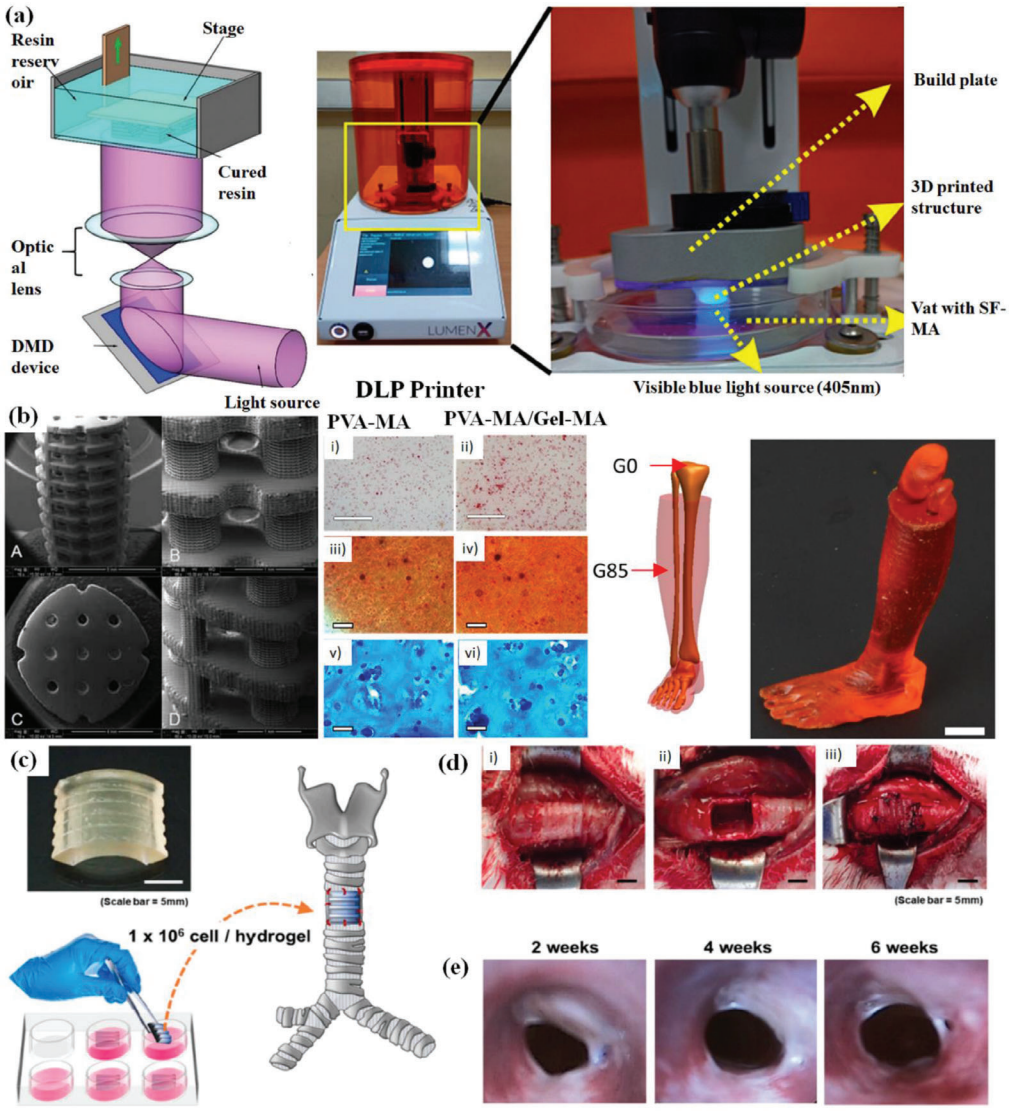

Figure 3. Printing mechanism and application of DLP technique. a) The schematic diagram depicts the operation of DLP-based 3D printing technology. Reproduced under the terms of CC BY 4.0 license.[33] Copyright 2020, The Authors, published by WHIOCE. And DLP printed SF-MA hydrogel. Reproduced with permission.[34] Copyright 2022, Elsevier. b) DLP-printed bone scaffold and staining of cells encapsulated in the PVA, GelMA-based scaffold. Reproduced with permission.[35,36] (left) Copyright 2012, Taylor and Francis Group, and (right) Copyright 2018, IOP Science. DLP-printed limb with soft muscle. Reproduced under the terms of CC BY-NC 4.0 license.[37] Copyright 2019, The Authors, published by American Association for the Advancement of Science. c) Application of DLP-based 3D printing in constructing artificial trachea; d) removal of part of the trachea and implantation of the artificial trachea; e) endoscopy images at 2, 4, and 6 weeks after trachea transplantation. Reproduced with permission.[38] Copyright 2020, Elsevier.

DMD, also utilized in overhead projectors, displays such binary patterns.[31]

The build time is the same, whether the entire available illumination field or simply a portion of it has been exposed. As a result, DLP processing speed is frequently represented as cm h^{-1}, or the structure's height (number of layers) per unit time. In addition, because the layer of resin being polymerized is usually at the bottom of the vat and not in direct contact with air, DLP is less impacted by oxygen inhibition than SLA. The light sources have quickly progressed from traditional lamps to modern light-emitting diodes (LEDs), covering a wavelength range from deep UV to visible light. The number of pixels/mirrors provided by the DMD and the optics used to project the patterns onto the build platform determine the lateral resolution of DLP systems, typically in the range of 10–50 μm. The vertical resolution, or minimum layer thickness, is primarily determined by the light penetration depth into the material and the subsequent curing depth. Light-absorbing additives, such as naphthol-based dyes, can adjust vertical resolution while reducing the undesirable effects of dispersed light. For example, slurries containing ceramic or metal particles can be processed with DLP in addition to nonfilled photopolymers.[32] The photosensitive polymer matrix is a binder in this situation, whereas the fillers are typically photochemically inactive. **Figure 3**a depicts the operation

of DLP-based 3D-printing technology and the construction of SF-MA (methacrylated silk-fibroin) hydrogel through the digital light processing method. Figure 3b–e shows various DLP-printed structures' application and printability properties.

3.3. Continuous Liquid Interface Production (CLIP)-Based Printing

CLIP is a type of vat photopolymerization AM pioneered by DeSimone et al. that uses an oxygen-permeable membrane to limit polymerization at the surface close to the UV source, eliminating the requirement for an intermediary recoating phase.[39,40] CLIP technique is an advanced technique of DLP. The CLIP technique's core premise is simple: UV projection at the bottom causes the photosensitive resin to harden, while the liquid resin at the tank's bottom Figure 2b maintains a steady liquid due to oxygen inhibition, assuring curing continuity. Light and oxygen can pass through a unique window at the bottom. The technology's main benefit is that it can be used to build objects in a disruptive way—25 to 100 times faster than a DLP 3D printer, with a theoretical printing rate of 1000 times that of the DLP approach and stratification that can be endlessly fine. The current method of 3D printing necessitates cutting the 3D model into multiple layers, comparable to the superposition of slides, which leaves the roughness unavoidable.

CLIP has significant advantages over other versions of SLA, and the business Carbon 3D, Inc., which sells instruments, materials, and services, has commercialized it. On the other hand, the CLIP approach allows for continuous change in image projection, akin to a slide growing into a superposition video, and this is a significant step forward from DLP projection technology.[41]

CLIP is significantly faster than standard DLP since the resin recoating step is the most time-consuming operation of the DLP lithography process, allowing the creation of objects with features less than 100 m at the z-axis growth rates of 30 cm h^{-1}. A CLIP device is similar to a DLP device except that it does not have a motorized stage and instead has an UV and oxygen-permeable glass at the bottom of the vat. The oxygen concentration at the bottom of the vat is high enough to generate a "dead zone" in which radical polymerization does not occur at rates exceeding 100 cm h^{-1}; lower resolution objects can be grown. The curing depth can be calculated as follows

$$\text{Curing depth} = C\left(\frac{\varphi_0 \alpha_{\text{PI}}}{D_{\text{c0}}}\right) e^{-0.5} \quad (1)$$

where C denotes the oxygen permeability constant (30 for a 100 μm thick Teflon AF film with air on the underside), ϕ_0 is the photon flux, and α_{PI} is the photoinitiator's absorption coefficient, respectively.

Although CLIP is a relatively new technology, Carbon 3D has been quick to produce commercial tools and better resins that allow the fabrication of things made of hard-to-elastic polymers and ceramics.[42,43] For rapid and precise CLIP, a dead zone thickness of 20–30 μm was ideal. Crosslinking occurs in areas illuminated by the imaging unit just above the dead zone. Increasing the concentration of a passive light absorber improves feature resolution in the z-direction. Lowering the absorber concentration allows for greater light penetration and, as a result, faster production.

4. Photopolymerization: Manufacturing Technology and Design

4.1. Mechanism of Photopolymerization

4.1.1. Radical Polymerization

Free radical photopolymerization is a commonly utilized technology for preparing polymeric materials, especially when its distinctive characteristics (spatial resolution and process precision) are critical. (Meth)acrylate monomers/oligomers are often used for 3D photopolymerization techniques that utilize radical systems. Radical systems include the fundamental processes of radical production, initiation, and propagation. Under light irradiation, radical production (in photopolymerization) is incurred. Under light irradiation, the Norish type 1 cleavage reaction is performed by the most commercially available photoinitiators to yield radical fragments.[44–46]

The incident light required to cause cleavage varies in wavelength and intensity depending on the chemical structures of the photoinitiator. Benzyl ketals with relatively low energy $n\rightarrow\pi^*$ transitions, such as 2-hydroxy-2-methyl-1-phenyl-propane-1-one (Irgacure 1173) and 2,2-dimethoxy-2-phenyl-acetophenone (DMPA; Irgacure 651) absorb light in the UV spectrum, making them appropriate for SLA-based process. Phosphine oxide photoinitiators have a lower energy level of the π^* state, which shifts the peak of the $n \rightarrow\pi^*$ transition to higher wavelengths, making them better suited for DLP-based systems.[44] Two-component photoinitiating systems consist of an uncleavable sensitizer and a co-initiator (known as type II), creating exciting triplet states under light.[47] Cam-phorquinones (CQ), benzophenones, and thioxanthones are the most often utilized uncleavable photoinitiators because they can undergo hydrogen-abstraction or electron-transfer processes in the presence of co-initiators, such as tertiary amines.[45] In the case of photocurable resins, a combination of radical photoinitiators can be used.

4.1.2. Thiol-Ene Addition

Thiol reactions involving reactive carbon double bonds, or "ene," are well-known. Michael-addition reactions or radical step-growth polymerization also fall under this mechanism.[48,49] These reactions can take place in a variety of ways. Photocurable polymers based on thiol-ene have advantages over formulations based on (meth)acrylates. For example, molecular oxygen inhibits the propagation of carbon radicals. In the resin, it is dissolved.[50] The difficulty is made worse because the curing surface is in constant touch with ambient air in open vat SLA installations. Traditional oxygen inhibition inhibitors, such as tertiary amines and retard cationic polymerization, are unsuitable for combined epoxy/polymerization. The chemistry of "thiol-ene" was one of the first alternative monomer systems studied for SLA.[51] In this case, the thiol-ene component is a dinorbornene, created by Diels–Alder cycloaddition of a diacrylate (different diol acrylates, including hexanediol diacrylate) to cyclopentadiene. In an equimolar ratio with a polythiol, the formulation cures significantly less radiation than DGEBA DA (diglycidyl ether of bisphenol-A diacrylate) (2 mJ cm^{-2} vs 13 mJ cm^{-2}). The DGEBA

DA attributes a weak response to oxygen inhibition.[52] By contributing a hydrogen atom to a generated peroxyl radical and creating reactive thiyl radicals in the process, thiols can reduce oxygen inhibition. Compared to acrylate-based formulations, thiol-ene-based formulations have less polymerization shrinkage and lower shrinkage stress. Thiol-containing acrylate/methacrylate-based resins shrank substantially less during photopolymerization than those without, resulting in crisper structures. Compared to (meth)acrylate-based networks, thiol-ene systems have superior biocompatibility.[53] Because of these advantages, thiol-ene chemistry has become a popular method for creating biocompatible and biodegradable hydrogel constructions, optical waveguides, and woodpile photonic crystals.[54–56]

4.1.3. Thiol-Yne Addition

Thiol-yne chemistry is made possible by adding alkyl thiols to carbon–carbon triple bonds. A vinyl sulfide is a chemical intermediate that can be added again with extra thiol. Compared to thiolene-derived products, this reaction generates a more extensive crosslinked network, resulting in a more excellent glass transition and mechanical properties.[57,58] Griesser and colleagues, e.g., generated alkyne carbonate derivatives (e.g., 2,2-bis [4-(2-hydroxy)ethoxyphenyl] propane dibut-3-yn-1-yl carbonate or 1,4-butanediol dipent-4-yn-2-yl carbonate) as biocompatible and biodegradable building blocks for a thiol-yne photopolymerization, which was started in a DLP printer with blue light (465 nm) irradiation.[53] 3D-printed products based on tricyclodecane-carbonate of 4,8-dimethanol dibut-3-yn-1-yl demonstrated polylactic acid-like rigidity (as a polymeric implant material, the thermoplastic biopolymer is widely employed). The cytotoxicity of this system was likewise lower than that of the equivalent (meth)acrylates.[53]

4.2. Photoinitiators Affecting Printability

The right photoinitiator is critical to ensuring a desirable polymerization rate and optimum functioning for biomedical applications.[59] On the other hand, using cationic photoinitiators would create protonic acids, which could damage cells, severely limiting their applicability.[41] Both radical and cationic photopolymerization processes exist. Based on their mechanism in the formation of free radicals, radical photoinitiators are split into two types: photoinitiators that are photocleavable (type I) and biomolecular (type II). Photoinitiators of type I, such as benzoin and acetophenone derivatives, have been widely utilized.[42] When exposed to light, type I photoinitiators absorb input photons and degrade into two prominent radicals, which activate the photocrosslinking reaction. Camphorquinone, thioxanthone, and benzophenone are type II photoinitiators that take hydrogen from the co-initiator to form secondary radicals for crosslinking.[43] Initiation happens when photolytic energy is converted into reactive species by the photoinitiator or photoinitiation mechanism under the influence of light. Xenon lamps, mercury arc lamps, LEDs, and lasers can be the light source. Photon sources can be utilized at wavelengths of 190–400 nm (UV), 400–700 nm (visible light), or 700–1000 nm (IR region).[13] An overview of some commonly used photoinitiators used in photopolymerization is shown in **Figure 4**. The following section summarizes the photoinitiating systems for 3D-printing applications described in the literature.

4.2.1. UV Light-Sensitive

In 3D-printing applications, various UV-light-sensitive photoinitiators that are commercially available are employed.[60–63] Hull's first photocurable materials included benzophenone as a photoinitiator for SLA application, activated using a photon source of 350 W mercury short arc lamp. To cure resins that absorb at 325 nm, this work was expanded with a more effective photon source (He-Cd laser).[44] Chiaponne and colleagues utilized two different photoinitiators: bis (2,4,6-trimethyl benzoyl) diphenylphosphine oxide (Irgacure 819; BAPO), which has a deep blue to near UV absorption, and Irgacure 1173, which is UV-sensitive, to start the photopolymerization of PEGDA in a DLP process.[64] The photopolymerization of PEGDA was performed with Irgacure 819 as a crosslinker and silver nanoparticles with a DLP system.[65] An enhanced electrical conductivity has occurred in thermally treated 3D-printed structures through in situ production of silver nanoparticles.[65] The photoinitiator (VA-086) has been used in biocompatible 3D-printing systems with less cytotoxicity and a more significant absorption peak (375 nm).[66] Irgacure 651 (DMPA) is another water-soluble photoinitiator employed in various 3D-printing systems, including creating biocompatible hydrogel scaffolds with fractal topologies.[67] Diphenyl-2,4,6-trimethyl benzoyl-phosphine oxide (Darocure TPO) is another UV-sensitive photoinitiator.[39,60,68] Lee and colleagues recently reported the possibility of employing a Darocure TPO photoinitiator for SLA-based 3D printing.[69] Although developed as an UV photoinitiator, it can absorb light up to 420 nm, which was sufficient to produce radicals under visible light irradiation (>400 nm) and promote 1,6-hexanediol diacrylate and pentaerythritol tetra-acrylate photopolymerization. Because Darocure TPO is colorless, it can be used to create 3D structures with optical transparency. 3D-printed structures with high mechanical toughness are typically nontransparent or partially transparent, whereas 3D objects with high optical transparency are typically PEG-based and have soft mechanical qualities, limiting their potential bio-applications in tissue engineering. Compared to the standard 3D hydrogel objects generated using Irgacure 2959, the printed constructs employing Darocure TPO displayed high transparency and mechanical qualities. Some photopolymerization reactions necessitate the use of more complicated photoinitiating systems. In an SLA-based 3D-printing system, e.g., a mixture of components was necessary to commence the photopolymerization of PEGDA resin mixed with cellulose nanocrystals (laser at 405 nm).[70] The photoinitiating system combines disodium (3Z)-6-acetamido-4-oxo-3-[4-(2-sulfonatooxyethylsulfonyl)phenyl]hydrazinylidene] naphthalene-2-sulfonate (RO16), lithium phenyl (2,4,6-trimethyl benzoyl)-phosphinate (LAP), and (2,2,6,6-tetramethyl 1-piperidinyloxy) (TEMPO) modified to absorb light at a longer wavelength than UV light.[70] The balance between biocompatibility and photon absorptivity was achieved when LAP was utilized to attain water solubility, while RO16 and TEMPO were used to control the

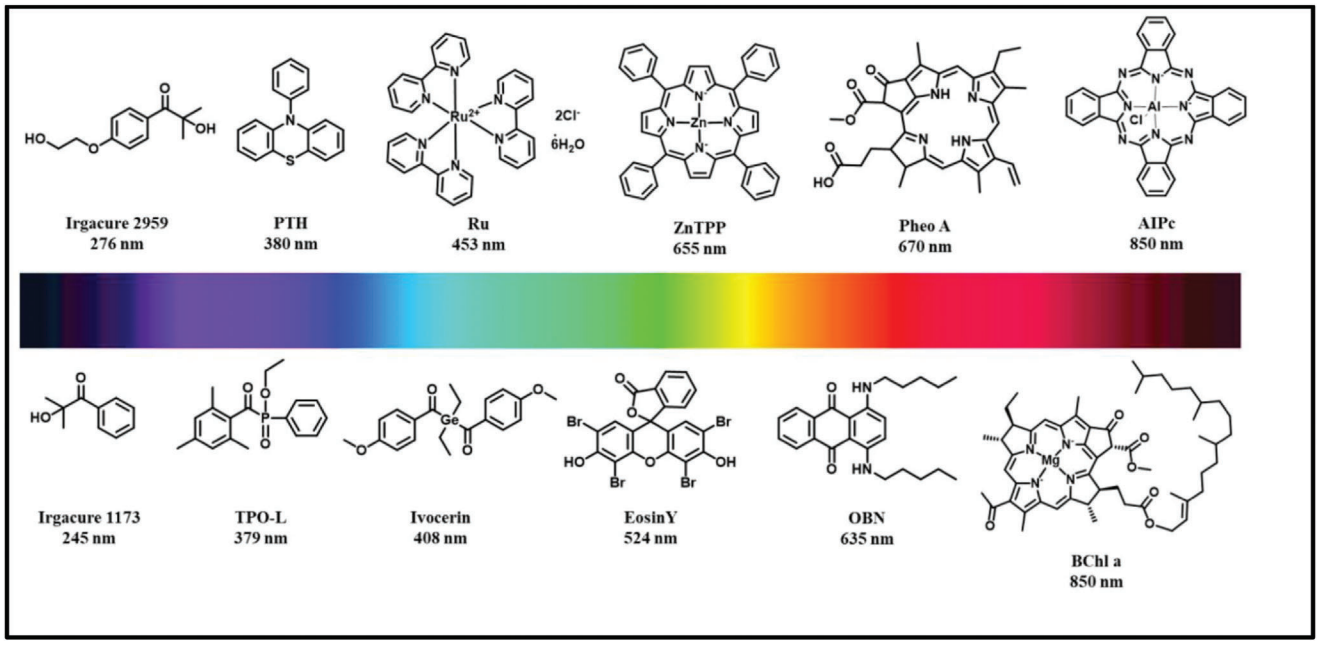

Figure 4. Examples of some UV light and visible light-sensitive photoinitiator/photocatalyst used in photopolymerization. Reproduced under the terms of the CC-BY license.[13] Copyright 2019, The Authors, published by American Chemical Society.

photopolymerization reaction. This technology can be utilized for tissue engineering and has been used to 3D print complex structures such as a human ear build.[70]

4.2.2. Visible Light-Sensitive

There has been much interest in polymerization under visible light irradiation.[71,72] Visible light can be used to get beyond the constraints imposed by high-energy UV light exposure while lowering the risk of eye injury. Visible LEDs are more environmentally friendly than UV light since they do not emit ozone and have a minimal thermal effect with long lives. Longer wavelength photons are also more gentle on live cells, making them ideal for biomedical and dental applications.[73–75] Due to these benefits, visible light in 3D applications has emerged by taking advantage of visible light-sensitive photoinitiators (**Table 1**).[73,76] To commence photopolymerization under visible light irradiation, Liska and co-workers used a bimolecular photoinitiator system consisting of CQ with visible light absorption and a tertiary amine such as ethyl 4- dimethyl-amino-benzoate. However, this approach has some drawbacks, including toxicity, the amine-based initiator's tendency to discolor, and low reactivity.[77] Alternative titanocene photoinitiators can absorb up to 560 nm; however, the system's applicability has been limited due to discoloration of the cured material (due to the photobleaching impact of the photoinitiators).[78] To imitate the 3D-printing process of cub flow resin, Liska, Stampfl, and co-workers used a 400 nm LED array to activate three different photoinitiators, including Ivocerin, BAPO, and TPO-L (a commercially available 3D-printing resin based on bi-functional methacrylates).[79]

These photoinitiators are ineffective under some LED sources with extended wavelengths because their absorption weakly tails out at 420 nm.[78] The usage of naphthalimide derivatives (1,8-naphthalimide derivatives carrying a methacrylate functional group) as light-sensitive photoinitiators was recently reported by Xiao et al.[90,91] Derivatives with an alkyl amine substituent at 4-position coupled with an iodonium salt, amines, N-vinyl carbazole (NVK), or 2,4,6-*tris*(trichloromethyl)-1,3,5-triazine are used to elicit radical or cationic photopolymerization under visible light (e.g., a laser diode (405 and 457 nm), blue LED bulb (462 nm), or soft halogen lamps. Compared to the photoinitiator systems of camphorquinone/amine and camphorquinone/iodonium salt, the reported combinations performed better.[90–92] Following these findings, to create reactive

Table 1. List of visible light photoinitiators employed in photocurable 3D printing.

Photoinitiators	Light absorption (λ)	References
Eosin Y	524 nm	[80]
Bis(4-methoxybenzoyl) diethylgermanium (Ivocerin)	408 nm	[81, 82]
Zinc tetraphenylporphyrin (Zn TPP)	420 nm	[83]
5-amino-2-benzyl-1*H*-benzo[de]isoquinoline-1,3(2H)-dione (NDP2)	417 nm	[74]
Camphorquinone (CQ)	468 nm	[84, 85]
2,6-bis(triphenylamine) thieno [3,2-b:2',3'-d] Phosphole oxide (TPA-DTP)	465 nm	[86]
3-nitro-9-octyl-9H-carbazole (C2)	375 nm	[80]
Tris (2,2-bipyridyl) dichlororuthenium[11] hexahydrate (Ru)	453 nm	[87, 88]
3-Hydroxyflavone (3HF)	350 nm	[89]

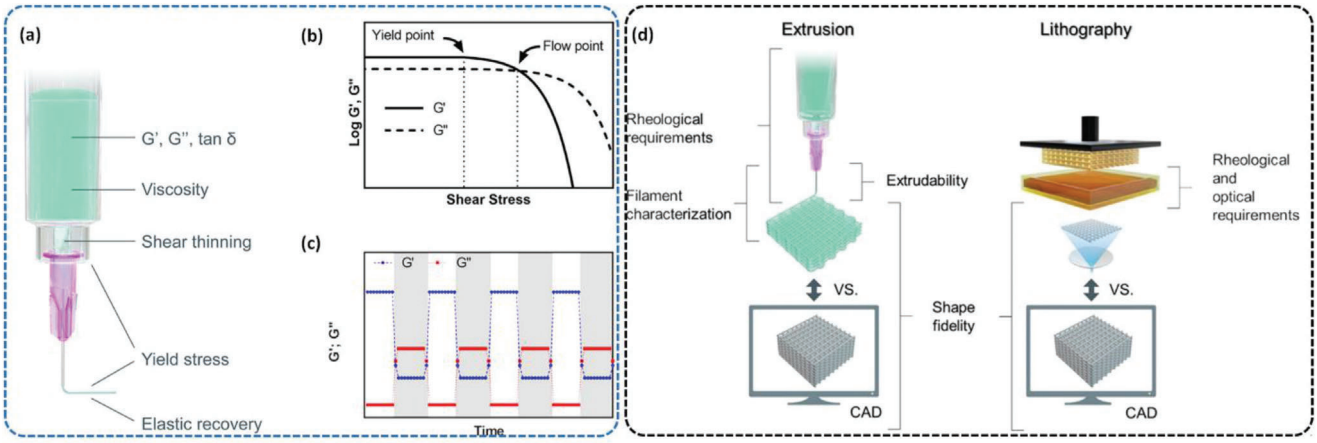

Figure 5. Rheological factors affect the printability of the photopolymer bioinks. a) An overview of the polymer ink extrusion process and rheological definitions; b) an example of an amplitude sweep test as a function of shear stress, demonstrating the yield and flow points of a given hydrogel ink. This can be measured as storage (G') and loss (G'') modulus with corresponding viscosity modulus; c) the hydrogel recovery test or elastic recovery test under low (white region) and high deformation (gray region) show the elastic recovery of an ideal printable hydrogel; d) critical aspects of assessing the printability of a photopolymer hydrogel ink during extrusion or lithography-based 3D-printing technology. Reproduced under the terms of the CC-BY-NC-ND license.[102] Copyright 2020, The Authors, published by American Chemical Society.

species (radicals or cations) under visible light irradiation, several naphthalimide derivatives were synthesized and coupled with an iodonium salt or an amine in two-or-multiple photoinitiating systems. Under various photon sources, these photoinitiating systems were successful in initiating the free radical polymerization of acrylates (TTA) or cationic polymerization of epoxides (EPOX) (including 385, 395, 405, 455, or 470 nm LED) or the polychromatic visible light from the halogen lamp. The NDP2 (5-amino-2-benzyl-1*H*-benzo[de]isoquinoline-1,3(2H)-dione, NVK, and diphenyl iodonium hexafluorophosphate were used to induce the radical (free radical) polymerization of tricyclodecane dimethanol diacrylate/triethylene glycol dimethacrylate (in the influence of air) utilizing a 3D printer with a 405 nm LED projector.[73] Organometallic photoinitiators (photo-redox catalysts) have been extensively utilized in laboratory investigations, whereas photoinitiators with organic structures are commonly used in commercial light-curing applications.[93] Intense absorption of visible light, regularly long-lasting excited states, and appropriate redox potentials are among the photochemical features of these metal complexes.[94,95] These compounds can operate as photo-redox catalysts (in either an oxidation or a reduction cycle),[96,97] generating active species and driving photopolymerization systems, including photo-induced atom transfer radical polymerization, photo-induced reversible addition-fragmentation chain transfer, and others.[98–100] The photoinitiator system based on copper complexes with pyridine-pyrazole ligand (with relatively high absorption in the 350–600 nm range) is utilized as a photo-catalyst to initiate cationic polymerization of epoxides and radical polymerization of (meth)acrylates, under the LED irradiation of 405 nm.[101]

4.3. Rheological Parameters Affecting Printability

Rheological properties are the typical physicochemical parameters that profoundly affect the printability of a photopolymer hydrogel.[102] When a polymer hydrogel is extruded from the nozzle, it undergoes temporary shear stress (deformation). After being extruded from the printing nozzle, the hydrogel quickly retained its original shape (reformation). Therefore, any printable hydrogel exhibits an initial bulk resting phase, then a transition to a high shear condition, and finally recovered to a new resting phase.[102,103] The viscoelastic nature of the photopolymer hydrogel describing these transition phases could be defined as viscosity (η), visco-elastic shear moduli (G', G''), elastic recovery (η vs t), shear and yield stress, respectively (**Figure 5**a). Viscosity is defined by the ratio of the shear stress to the corresponding shear rate. A typical fluid showing a linear relationship between shear stress and shear rate is defined as *Newtonian* behavior. Conversely, any fluid showing the deviation from linearity, with either increasing or decreasing ratios is termed as *non-Newtonian* behavior. The *non-Newtonian* behavior of hydrogels can be classified into two categories:[1] time-independent fluids (shear-thinning and shear-thickening) and[2] time-dependent fluids (thixotropic or rheopectic).[104]

4.3.1. Shear-Thinning and Thickening Hydrogels

It is the most common type of fluid behavior, where increased shear stress decreases viscosity. This property is usually used in extrusion-based 3D printing of polymeric hydrogels, polymer solutions, partially crosslinked hydrogels, and colloidal suspensions.[102] In extrusion or DLP-based 3D printing, shear-thinning is connected to the initial shape preservation of any polymeric hydrogels, with a gradual decrease of viscosity during the extrusion through the nozzle. However, the shear forces dramatically increase. After the shear stress is removed, the viscosity gradually increases, thereby contributing to preserving the printed shape. Therefore, the higher the zero-shear viscosity, the more excellent the printability of the printed constructs for ceramic-based nanocomposite hydrogels.[102,103,105] The actual

mechanism behind this phenomenon is closely connected to the polymer structure and degree of precrosslinking. When a shear-thinning hydrogel is extruded from the nozzle, it induces an initial disentanglement of the polymer chains. As a result of that, the polymer undergoes a critical sol–gel transition. The high shear stress allows the polymer chain to disentangle and align to minimize the internal resistance, followed by a change in viscosity.[106] Another type of time-dependent fluid is shear-thickening fluid or *non-Newtonian*, characterized by an increase in viscosity with increasing shear rate rather than a shear-dependent manner. Hydrogels showing this property are not generally relevant for 3D-printing applications.[102,106]

4.3.2. Viscoelastic Property Affecting Print Fidelity

Hydrogels extruded from the nozzle exhibit both flow and shape retention properties. During 3D printing, the hydrogel ink should flow properly with minimum internal resistance with or without cells. Therefore, the property of showing viscous flow and elastic shape retention is known as viscoelasticity.[103] Two types of shear moduli can explain this phenomenon:[1] storage or elastic moduli (G') and[2] viscous or loss moduli (G''), respectively. The storage modulus measures the energy stored elastically during a hydrogel deformation and is connected to the elastic shape retention property. The loss modulus is the amount of energy dissipated by the hydrogel connected to the viscous flow. Therefore, a ratio of G''/G' is considered a damping factor or loss factor or Tan (δ) value for a given hydrogel ink (Figure 5b). The yield stress or yield point is another phenomenon that indicates the maximum stress to be exceeded for the active deformation of a hydrogel ink.[103,107] Thus increased yield point usually improves the filament formation and shape fidelity of the target construct, but it can also affect the cell encapsulation. Branched polysaccharides, such as gellan gum, hyaluronic acid (HA), alginate, or carrageenan, are typical examples of hydrogel where the increasing concentration of the polymer grammatically increases the yield stress of a given ink.[102] Therefore, it is crucial to choose the appropriate concertation of the prepolymer concentration to obtain moderate yield stress, both for 3D printing and cell encapsulation (Figure 5c). An overview of the rheological factors and printability optimization for polymeric bioink is schematically represented in Figure 5d.

4.4. Computational Simulation and 3D Printing

The quantitative analysis of the photopolymer hydrogels after 3D printing is always challenging due to difficulty in the printed construct's actual dimensions and is mainly done by trial and error. Therefore, the printing parameters must be tuned graphically to obtain a proper 3D bioprinting procedure (from fabrication to post-processing). Recent studies indicate that good printability with proper bioink formulation often requires support from mathematical and computational models or theories to interpret more accurately.[108] Biological tissues exhibit complex micro/nanoarchitectures, which are difficult to print or even challenging to evaluate the shape retention property after 3D printing. Therefore, there is an immediate need for advanced engineering toolkits for evaluating the printing quality and post-processing of the fabricated bioink. This can be resolved by integrating two parameters:[1] Construction of patient-specific biomimetic structures from medical imaging data has enabled precise identification of the structure of target organs or tissues, and[2] high-resolution computerized fluid dynamics (CFD) simulation model that can define or illustrate the nature of anatomical variations, mechanical forces, and final shape retention properties.[108,109] Shafiee et al. reported a unique CFD-based 3D-printing technique known as cellular particle dynamics (CPD), where the particle type bioink fused to form a complex multicellular architecture through shape-changing biomechanical relaxation.[110] This technique is comparatively simple, more predictive, reproducible, and thus less time-consuming. The cylindrical bioink was rapidly deposited onto the platform containing multicellular spheroids and later fused to form a cylindrical tube-like structure (**Figure 6**a). After the fusion, the CPD model was used to evaluate and predict the tube formation dynamics (Figure 6b). In another study, the cardiac vessel's hemodynamic flow (Figure 6c) was predicated as a Newtonian fluid model using CFD simulation before 3D printing.[109] Therefore, high-resolution CFD modeling with 3D printing would provide a new dimension in constructing complex biological architectures with high shape fidelity.

5. Photopolymers: Manufacturing and 3D Printing

5.1. Methacrylated Collagen (ColMA)

Collagen is an excellent wound dressing material because it is biocompatible, biodegradable, and cytocompatible.[111,112] However, due to the limited flexibility of the polymer, collagen hydrogels generated via self-assembly are not ideal for soft tissue regeneration.[113] Physicochemical crosslinking has produced a variety of collagen hydrogels, but the high toxicity of the crosslinkers used has limited their biomedical applications.[114] Photopolymerization using visible or UV light is a promising technology for producing collagen hydrogels with desirable mechanical properties, such as photo-curing time.[115–117] As a result, the mechanical strength of the resultant hydrogel can be adjusted, which influences the pharmacokinetic release parameters of drugs/proteins contained in the hydrogel.[118] The usage of visible light is safer than the use of UV light. Antimicrobial compounds, in addition to visible light-cured hydrogel systems, are wound healing accelerators. Triclosan, e.g., has broad-spectrum antibacterial activity and is low in human skin toxicity, although it has limited water solubility.[7,22]

5.2. Methacrylated Alginate (AlgMA)

Alginate methacrylate (ALMA), also known as methacrylated alginate and alginate methacrylamide, has long been utilized to make gels for application in biomedical disciplines.[119,120] Methacrylated alginate is made by replacing the carboxyl or hydroxyl groups in alginate with methacrylate groups in a chemical reaction.[121,122] With the addition of a photoinitiator and low-level UV light, an ALMA hydrogel is synthesized by free radical polymerization of the methacrylate groups.[119] Cova-

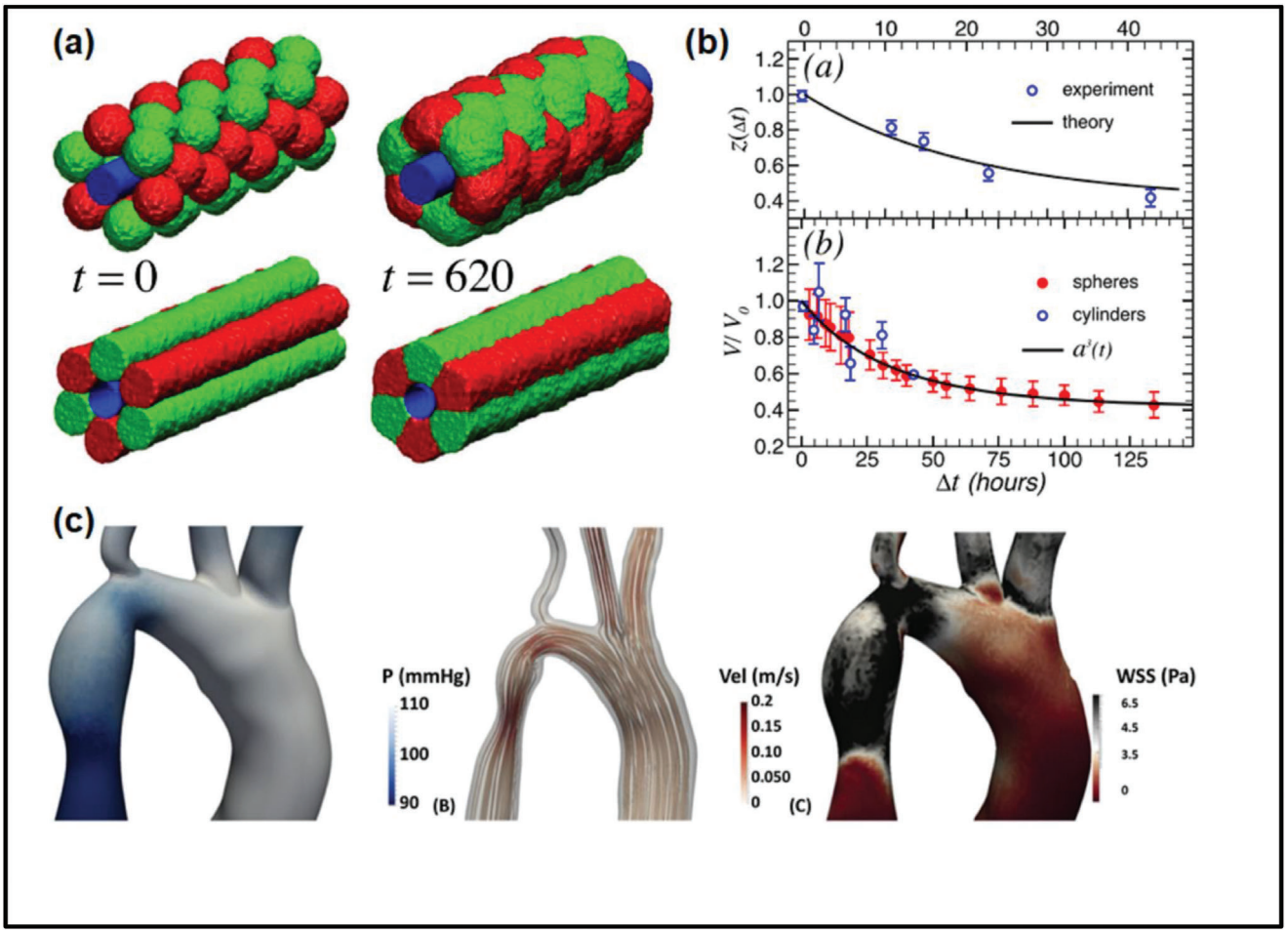

Figure 6. Computational modeling shows the flow ability of the printable hydrogel inks. a) Photographs showing the start and end of the CPD simulations of tube formation via controlled fusion of spherical aggregates. b) Relative change in length, $z\ (\Delta t) = L\ (\Delta t)/L_0$, versus time, $\Delta t = t - t_0$ of the cylindrical aggregates during the 3D printing process. Reproduced with permission.[110] Copyright 2015, IOP science. c) CFD simulation models show the hemodynamics of blood flow as a *Newtonian* fluid of a human aorta before 3D printing. Reproduced with permission.[109] Copyright 2017, Elsevier.

lent functionalization of the ALMA backbone with cell adhesive ligands such as RGD-containing peptides can easily endow ALMA hydrogels with cell adhesion.[123–125] Michael's addition process,[126] photocrosslinking,[125] and ordinary carbodiimide chemistry[123,127] have all been used to insert the RGD sequence into ALMA hydrogels. ALMA hydrogels with cell adhesion properties have been shown to considerably stimulate the increased proliferation and growth of osteoblast-like cells and adult stem cells.[114,125] Because some biopolymers, including gelatin and collagen, include the respected sequence in their molecular structures, using these biopolymers in combination with ALMA hydrogels provides an alternative, less expensive way to introduce the RGD sequence.[128,129] It has been established that adding collagen to the ALMA matrix can considerably promote osteogenesis, due to its potential to increase the mechanical scaffold qualities and its intrinsic property of boosting cell adhesion and activating signaling pathways toward higher osteogenesis.[129,130] In addition to biomaterials, growth factors and other biomolecules have been put into ALMA hydrogels to promote osteogenesis. BMP-2 has been used with other hydrogels, including ALMA hydrogels known to stimulate osteoblast development.[123,128]

Furthermore, due to their physical qualities, other biomaterials with the required properties can be easily mixed with ALMA to create a biocomposite scaffold that promotes bone repair. Furthermore, their crosslinking methods enable the creation of scaffolds with microstructures that can precisely contain specific cell types, resulting in a better expressivity of bone markers.[131]

5.3. Methacrylated Hyaluronic Acid (HAMA)

HA is a biocompatible nonsulfated glycosaminoglycan made up of repeated *N*-acetyl glucosamine and D-glucuronic acid disaccharide units standard in tissues such as cartilage, neurons, and skin.[132] HA contains hyaluronidase target sequences that can promote cellular microenvironment modification,[133] as well as the ability to interact precisely with CD44 and CD168 (hyaluronan receptors), heavily expressed by most tumor cells.[134] However, HA hydrogel's mechanical characteristics are poor, degrading quickly,[135] restricting its usage in biomedical applications. HA methacrylation is required to produce optimal mechanical properties and control degradation rate,[135,136] making HAMA

hydrogel appropriate for various biological applications, such as cell therapy, tissue regeneration, medication administration, and biosensing.[134,137,138] The HAMA prepolymer solution is made by methacrylating HA (by substituting volatile amine and hydroxyl units of HA by methacryloyl units) using demineralized water with the pH range between 8.0 and 8.5 (at 4 °C).[134,139] The prepolymer solution is then dialyzed for 2–3 days using dialysis tubing with molecular weight cut-offs ranging from 6 to 8 kDa to eliminate all MA byproducts and unreacted MA.[134] Finally, the dialyzed solution is freeze-dried to create HAMA prepolymers. Under the exposure of Irgacure 2959 and UV irradiation, 0.25–4.0% w/v of prepolymers could be employed to manufacture HAMA hydrogel constructions using various microfabrication techniques (such as electrospinning, micromolding, and bioprinting).[140,141] Adjusting the prepolymer concentration or light exposure period can alter the mechanical properties of HAMA hydrogel.[142,143] For example, increasing the prepolymer concentration from 1% to 3% w/v raised the elastic modulus of HAMA hydrogel from 1.3 to 10.6 kPa.[141] Apart from mechanical qualities, the prepolymer concentration of HAMA hydrogel can be tweaked to alter the rate of degradation. 24 h followed by incubating in hyaluronidase mixture, enzymatic breakdown of HAMA hydrogel reduced from 100% to 50% when the prepolymer content was increased from 1% to 3%.[143] For cell remodeling in 3D tissue-engineered construct, high degradability of HAMA hydrogel is essential.

UV light crosslinked HAMA hydrogels were utilized to build 3D in vitro central nervous system (CNS) normal and pathological tissue prototypes for the study of neurological diseases and regeneration because HA is a critical extracellular matrix (ECM) component for CNS development.[141] HAMA hydrogels have also been employed to create bone and cartilage tissue constructs for osteoblast and cartilage repair, respectively.[143] Incorporating other organic or inorganic components into HAMA hydrogel can increase its mechanical and chemical properties, further improving its functionality. Combining HAMA hydrogel with pure matrix peptide for nerve healing may increase neurite extension or outgrowth.[144] HAMA hydrogels have also been electrospun into aligned nanofibers and supplemented using poly-lactic-*co*-glycolic microspheres to regulate the secretion of nerve growth factors for peripheral nerve repair and regeneration.[140] HAMA hydrogels containing damaged cartilaginous microscopic particles, methacrylated chondroitin sulfate, or cadherin mimicking protein encapsulate cells (chondrocytes or mesenchymal stem cells) have higher levels of cartilage markers and collagen type II deposition compared to cells encapsulated in pure HAMA hydrogel.[134,143,145] Furthermore, the GelMA/HAMA composites create 3D in vitro cardiac tissue structures to better understand the fibrotic remodeling and calcification processes in heart valve illnesses.[142,146,147]

5.4. Methacrylated Gelatin (GelMA)

Gelatin is a food-processing substance that the Food and Drug Administration has approved. Because of its biodegradability, biocompatibility, and low antigenicity, it is a popular hydrogel foundation material.[148,149] Gelatin is a collagen hydrolysis product that comprises numerous arginine-glycine-aspartic acid (RGD) sequences and matrix metalloproteinase target sequences that increase cell adhesion and cellular microenvironment modification, respectively.[150,151] On the other hand, gelatin hydrogel degrades quickly and has low mechanical strength, limiting its biological applications. In 2000, hydrogel in which gelatin is complexed with methacrylate groups (GelMA) was introduced.[152] The methacrylation technique has slowed gelatin deterioration and increased its mechanical strength .[153,154] GelMA hydrogel is therefore suited for a wide range of biological applications, including tissue engineering and regenerative medicine, as well as medication, growth factor, and gene delivery.[128,155,156] For cartilage and tooth regeneration, UV light-crosslinked GelMA hydrogel has been employed to build tissue-engineered cartilage- and prevascularized dental pulp-like constructions.[157] 3D-bioprinted chondroprogenitor cell-laden articular cartilage GelMA hydrogel was proven to be highly effective than the hydrogel-containing mesenchymal stem cells (MSCs) or chondrocytes in nonhypertrophic neo-cartilage production.[157] GelMA hydrogel has also been utilized to create in situ 3D structures such as blood clotting and cardiac (fibrotic cardiac) tissue constructs to research fibrotic remodeling and thrombosis, respectively.[158,159] It has also been used to develop a platform for toxicology testing the drug based on organ-on-a-chip (e.g., acetaminophen toxicity).

Furthermore, in mouse spinal cord transection models, the implantation of GelMA hydrogel-encased neural stem cells (NSCs) was reported to improve neuronal regeneration and reduce glial scar formation, implying that the construct could be used to treat spinal cord injury.[160] Nanosilicate-customized GelMA hydrogel with vascular tissue in the presence of osteoinductive and vascular-endothelial growth factors (VEGF) enhances the bone mineralization and osteogenic potential of mesenchymal stem cells, implying that the vascularized 3D bone tissue construct can be utilized for bone tissue regeneration as bone transplants.[161] A blended bioink comprised of GelMA hydrogel, sodium alginate, and PEGTA can be used to print larger-scale and highly controllable 3D vascularized tissue structures, which has tremendous potential for tissue repair and regeneration.[146,162]

5.5. Methacrylated Chitosan (ChMA)

Chitosan is the term given to a group of linear polysaccharides made up of β-1→4 linked D-glucosamine with some *N*-acetyl-D-glucosamine interleaved. Chitosan is the only natural polycationic polysaccharide, and it is soluble in the (slightly) acidic medium[163] because the pK_a of the amino groups is around 6.6 at 25 °C. Chitosan is available in good laboratory practices and good manufacturing practices (GMP)-compliant forms, combined with its biocompatibility and biodegradability,[164] making it an attractive polysaccharide for tissue engineering and biomedical applications.[165,166] Chitosan has been proposed for a variety of medicinal applications, including topical ocular applications,[167] implantation,[168] injection, and medication delivery.[169] Chitosan is bio-adhesive, a feature that determines the time it stays at the application site.[170] In the dental field, chitosan has already been used in a commercial dental adhesive to take advantage of its antibacterial properties. Chitosan is a highly flexible polymer that may be easily altered to give it unique physical, chemical, and biological properties.

Recently, the chemical attachment of methacrylate moieties onto the chitosan chain has been used to create rechargeable antimicrobial polyurethane coatings. A photocrosslinkable hydrogel made of chitosan modified with methacrylic acid and proneural rat interferon stimulates the differentiation of adult neural stem/progenitor cells into neurons.[171] Diolosa et al. tested a primer based on a natural polysaccharide, chitosan, coated with methacrylic acid moieties (Chit-MA70). Chit-MA70 had both hydrophilic and hydrophobic properties and the ability to interact chemically or physically with both the restorative material and the organic part of the demineralized tooth, making it an excellent candidate for improving sealing and extending the durability of dental restorations.[172] The methacrylate-modified chitosan (Chit-MA70) was able to locate at the dentine-restoration interface and infiltrate the dentine tubules. The effect of methacrylate-modified chitosan in the primer used for dental restoration was the most intriguing finding of their research. Although extensive research on the modified chitosan's performance is needed, it could be an exciting component to add to water-based adhesive systems to improve the longevity of dental restorations.[173] **Table 2** summarizes the properties of various photopolymers and their characteristic features for tissue engineering and regenerative medicine.

6. Biomedical Applications

6.1. Application in Bone Tissue Engineering

Bone is a highly sophisticated biological tissue that can self-repair—inflammatory, reparative, and remodeling are stages of bone healing.[190] Chitosan is made from chitin that has been deacetylated.[191,192] Chitosan is widely available and inexpensive to produce.[169] Chitosan-based polymers are effective biomaterials for bone regeneration and tissue engineering applications. Chitosan methacrylate (ChMA) is frequently employed for 3D printing to create 3D constructions because of its intriguing features, such as injectability, cell deliverability, and fluidity. These biopolymer-based scaffolds can benefit from adding nanosilicate-based materials, improving biomineral formation. Laponite, e.g., is a multilayer synthetic silicate used to improve biopolymers' mechanical, dynamic, and biological properties. The osteogenic stimulator laponite is a nanopowder and can be used in the matrix as a bone growth stimulator.[193–196] **Figure 7** depicts the modification and application of several biopolymer scaffolds for the regeneration of bone tissue. In a study by Cebe and co-workers, biopolymers such as gelatin and chitosan were methacrylated and tuned to increase their network formation and limit hydrolytic degradation. The methacrylation was performed to improve the scaffolds' thixotropic properties and mechanical properties. To improve gelation, the methacrylated biopolymers were combined with a nanosilicate powder (laponite) to enhance the scaffold's compressive strength.

A rheometer was used to test the rheological properties of these polymer inks. For in vitro evaluation, 3D-printed mesh-like scaffolds were printed with these inks using a 3D printer. The gelatin- or chitosan-based materials were compared for their comparative impact on biomineral formation. Several factors have been attributed to the enhanced biomineral formation after 21 days of culture of MC3T3 cells when tested with methacrylated gelatin (MAG), methacrylated gelatin-laponite (MAG-Lp), methacrylated chitosan (MAC), methacrylated chitosan-laponite (MAC-Lp). Based on the increased affinity of chitosan to enhance cell growth, it was found that using chitosan methacrylated nanosilicate-based biomaterials could enhance the formation of minerals in osteoprogenitor cells, increase calcium-phosphorous mineral content, as well as mineral nodules in a short amount of time compared to gelatin-based scaffolds.[198] The chitosan has shown the ability to facilitate higher levels of cell growth, a higher phosphate-to-amide ratio, and the presence of calcium-phosphate biomineral nodules on the surface of the scaffold.

6.2. Application in Cardiac Tissue Engineering

3D bioprinting has also been utilized to create calcific aortic valve disease (CAVD) modeling in 3D that accurately reproduce leaflet layer biomechanics.[199] The healthy aortic valve (AV) comprises three semilunar leaflets, each of which has three stacked layers and a distinct ECM composition. The AV leaflet becomes calcified and fibrotic as the interacting cells of valve interstitial cells (VICs) undergo myofibrogenic and osteogenic development with the progression of CAVD.[200] Van der Valk and colleagues used lithium phenyl-2,4,6-trimethylbenzoylphosphinate photoinitiator to UV crosslinked a CAVD prototype containing 10×10^6 cells mL^{-1} of hVICs (human valve interstitial cells) in methacrylated HA (HAMA)/GelMA hydrogels for improved cardiac function.[199] The scientists also measured the compressive mechanical characteristics of each of the AV leaflet layers in this investigation, discovering that the ventricularis had Young's modulus of 26.9 kPa, which was halfway between the fibrosa and layers of spongiosa (15.4 and 37.1 kPa, accordingly, **Figure 8**a–e). The findings of their study have generated a fresh 3D model for the study of valve mechanobiology for the first time, and they can also make high-throughput drug screening for CAVD more feasible in a biologically appropriate context (Figure 8f,g). There have been a few reports of patient-specific 3D printing usage in cardiology preoperative training. The osteogenic agents were added to the 3D-printed hydrogels with encapsulated VICs to encourage microcalcification production (Figure 8h). The formation of microcalcific nodules was efficiently induced by exposure to osteogenic stimuli for 14 days; however, low amounts of apoptosis were detected in the encapsulated cells (Figure 8i), implying that calcification was independent of cell death by apoptotic processes. Gaetani and colleagues employed the pressure-based extrusion approach to 3D print a cardiomyocytes progenitor cells (CMPCs) patch of adult cardiac tissue (3×10^7 cells mL^{-1}) onto an alginate scaffold with controlled pore size and microstructure.[201] The cardiogenic potential of this patch was assessed by 7 days post-printing mRNA activation of the early cardiac transcription factors NK2 homeobox 5 (Nkx2.5), Gata-4, and myocyte enhancement factor 2C (Mef-2c), and the late cardiac marker troponin T (TnT) by these cells. The printed cells were further capable of transitioning from the matrix of alginate to the film of matrigel, resulting in tubular-like structures. In another study, the same team bioprinted a cardiac patch made up of adult CMPCs (3×10^7 cells mL^{-1}) embedded in a framework comprised of HA and gelatin, which was then used to treat 10–12

Table 2. A comparative table of various photopolymers and their application in tissue engineering and regenerative medicine.

Photopolymer	Synthesis	Printing method	Properties	Mechanical Features	Effects	Application	Refs.
ColMA	Reaction of methacrylic anhydride with the primary amino group present in gelatin	Digital light processing	Thermoreversible, self-assembled fibril formation,	Improved storage modulus and stiffness	Improved mineralization and cell viability	Cartilage repair, vascular regeneration	[174–177]
GelMA	Replacement of lysine and hydroxylysine with methacrylic anhydride	Extrusion-based direct-write 3D printing, electrospinning	Biocompatible, minimal invasiveness, reversible and nonreversible solidification thermosensitive	Enhanced storage modulus, greater compressive strength, maintain zero-shear viscosity	Increased mineralization and promote angiogenesis	Bone tissue engineering, skin regeneration, tendon regeneration	[178–181]
AlMA	Chemical alteration of carboxyl and hydroxyl group of alginate with methacrylate	Fused-deposition modeling, photoligraphy	Highly adhesive, biocompatible, anti-inflammatory, improved penetration into pore structures	Improved tensile and compressive modulus, Highly conductive	Increased expression of collagen II, SOX9, aggrecan, and collagen X, enhanced osteogenic and vasculogenic expression	Cartilage tissue regeneration, Bone regeneration	[114, 131, 182]
HAMA	Substitution of a hydroxyl group of hyaluronic acid with methacrylate	Extrusion-based printing	Highly photo-crosslinkable, enhanced cell attachment	Increased storage modulus and stiffness	Formation of stable printed structures, enhanced fibrocartilage formation, collagen II, and glycosaminoglycan content	Cartilage regeneration, cardiac tissue engineering	[183–185]
ChMA	Esterification of the hydroxyl group of chitosan with methacryloyl chloride	Extrusion-based 3D printing	Excellent biodegradability and biocompatibility, antibacterial properties	Enhanced compressive strength and storage modulus	Spread morphology of BMSCs, increased cell proliferation	Bone regeneration, wound healing	[186–189]

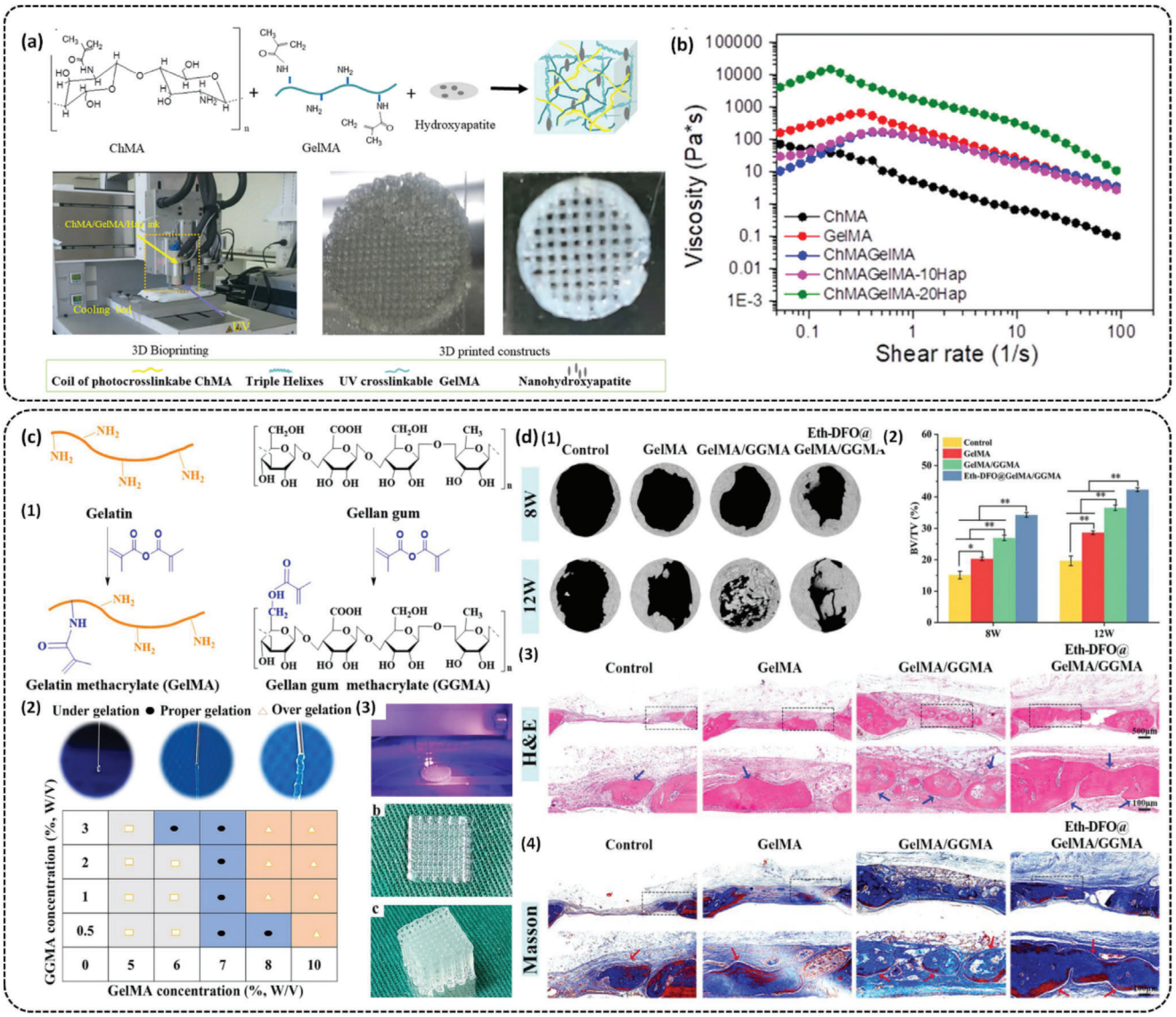

Figure 7. Application of 3D printing for bone regeneration. a,b) Schematic illustration of synthesis and 3D printing of a hybrid photocrosslinked hydrogel based on methacrylated chitosan (ChMA), gelatin methacrylate (GelMA), and nanohydroxyapatite (HAp) for bone regeneration. The incorporation of HAp into ChMA and GelMA matrix improved the mechanical performance of the composite hydrogel ink. Reproduced with permission.[186] Copyright 2021, American Chemical Society. c,d) Fabrication of GelMA and gellan gum (GCMA)-based 3D printable hydrogels for vascularized bone regeneration. The composite hydrogel ink is shear responsive,[1] rapid hydrogel-forming,[2] and printable[3] with improved shape retention properties. The GelMA-GCMA hybrid scaffold showed improved bone regeneration potential[1] in a calvaria defect model via active biomineralization and increasing the bone volume[2] and vascularization.[3] Scale bar: 100 μm. Reproduced with permission.[197] Copyright 2022, Elsevier.

weeks old infarcted mice.[202] The scaffold was a powerful vehicle for cell viability, engraftment, and differentiation after 4 weeks of implantation, ultimately increasing mouse cardiac function.

6.3. Application in Neural Tissue Engineering

Hydrogels containing porcine, bovine, rat tail collagen, neural stem, and progenitor cells have been demonstrated to multiply and differentiate. A study by Sanz et al. assessed the efficacy of methacrylated collagen from a common fish, the Red Snapper, to be used as a biomaterial for 3D-bioprinting neural cells. The cell lines ReNcell VM and NSC-34 were employed in their research. ReNcell VM is a human neural progenitor cell line isolated from the ventral mesencephalon of a developing brain and immortalized with the retrovirus v-myc via retroviral transduction. NSC-34 is a mouse motor neuron-like cell line that can be generated in vitro from a fusion of motor neuron-enriched primary embryonic spinal cord cells and N18TG2 neuroblastoma cells. The extraction, characterization, and methacrylation of Red Snapper collagen and the optimization of conditions for cell seeding and encapsulation using unmodified collagen, thermally crosslinked collagen, and methacrylated collagen with UV-induced crosslinking, were all investigated in their study.[198] In

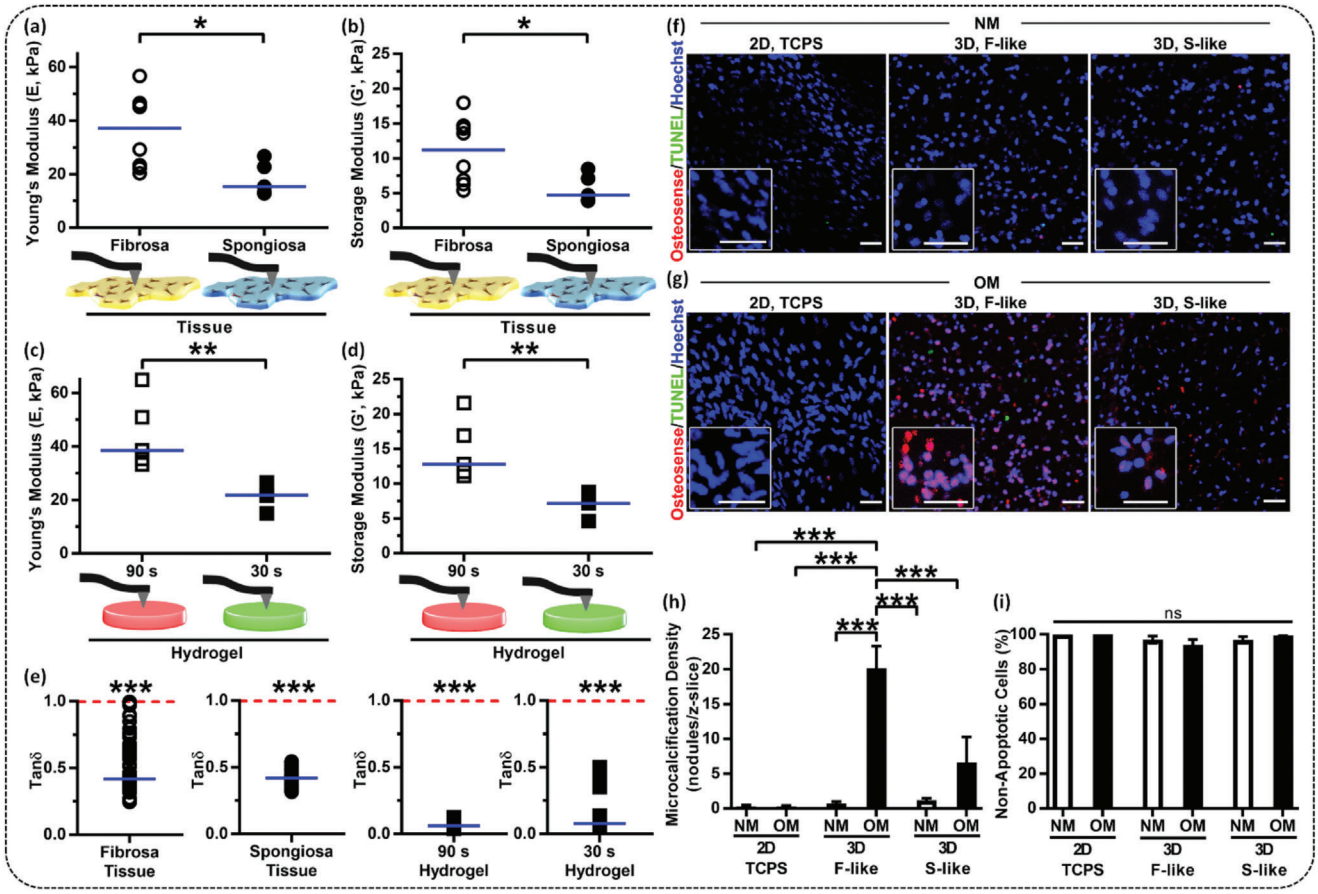

Figure 8. Application of 3D bioprinting for cardiac tissue engineering a–e) evaluation of the mechanical properties of the 3D bioprinted cardiac tissue constructs of GelMA-HAMA hybrid hydrogels; f,g) in vitro biocompatibility of the valvular interstitial cells (VICs) in the presence of GelMA-HAMA hydrogels. Scale bar: 50 µm; h,i) microcalcification and apoptosis assay of the VICs in the presence of GelMA-HAMA hydrogels. Reproduced under the terms of CC-BY license.[198] Copyright 2018, The Authors, published by MDPI.

their work, they constructed a structural NMJ (neuromuscular junction) model in vitro; skeletal myoblasts and motor neuron cells were co-axially bioprinted. The shell of bioprinted hydrogel strands was made from a bioink comprising fish collagen and motor neuron cells, while the core was made from a bioink containing myoblast-laden gelatin methacryloyl (GelMA) solution. Because distinct microenvironments surround myoblasts and motor neurons in situ, this specialized organization was used to help tune each bioink to the specific embedding cell type while merging them into a single ordered framework. The motor neuron cells were thought to stretch neurites from the shell layer to the core layer's periphery, where skeletal myoblasts had previously been found, generating motor neuron-skeletal muscle connections and NMJs.[203] They found that marine collagen isolated from the skin of Red Snapper fish can help neural cells survival and differentiation. For example, Schuh et al. engineered neural tissue using collagen-fibrin composites in vitro that supported Schwann cells and encouraged neurite development.[204] As a result, collagen composites that combine marine collagen with other polymers are more likely to provide improved conditions for neural modeling.

Using a 3D bioprinting approach, Lee et al.[205] created a collagen hydrogel with neural stem cells C17.2 (C17.2 NSCs) and vascular endothelial growth factor (VEGF). The C17.2 cells were found to have a vitality of over 92% after printing. As C17.2 cells were printed on a VEGF-fibrin gel, they showed significant morphological changes, multiplication, and migration compared to control cells. This method could help assess cellular behavior and nerve tissue regeneration. Owens et al.[206] used 3D bioprinting to make a cellular nerve graft. To begin, bio-ink components were produced from mouse bone marrow stem cells (BMSCs) and Schwann cells as cylindrical units. The nerve transplant was created by printing them in layers. In vivo testing has proven that cellular nerve graft restores both motor and sensory functions to certain levels as a result of the research. The bioprinted graft was found to be superior to an autologous transplant in the treatment of neurological injury in this study. A schematic illustration of polymeric scaffolds and their application for neural tissue engineering is depicted in **Figure 9**.

6.4. Application in Muscle Tissue Engineering

Skeletal muscle tissue accounts for 40–45% of an adult's body weight and is involved in locomotion, pretension, mastication, and body metabolic function.[211,212] It comprises bundles of par-

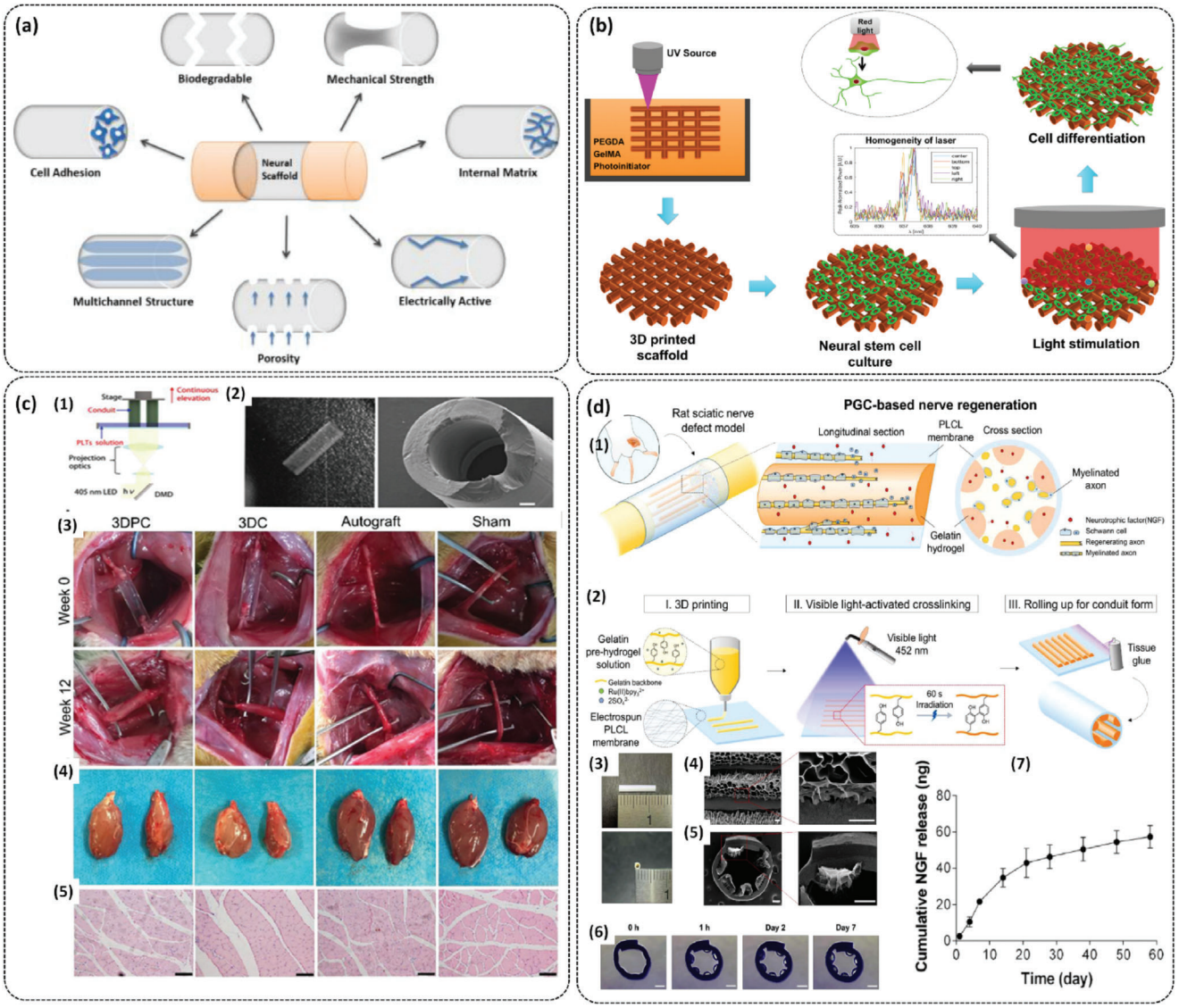

Figure 9. Application of photocurable polymers in neural tissue engineering via 3D printing. a) Schematic illustration for the selection criteria for a typical scaffold for neural tissue engineering. Reproduced with permission.[207] Copyright 2020, Elsevier. b) 3D printing of GelMA-PEGDA-based hydrogels with low-level light therapy for nerve regeneration. Reproduced with permission.[208] Copyright 2017, IOP Science. c) Fabrication of GelMA-based photocurable nerve conduits for peripheral nerve injury and repair. The DLP printing of polymer resin[1] and SEM morphology[2] of the designed nerve conducts. In vivo nerve regeneration test in a transected sciatic nerve showed complete regeneration[3–5] in the presence of the GelMA scaffolds. Reproduced with permission.[209] Copyright 2020, John Wiley and Sons. d) Visible light-activated PLCL-based printed nerve conducts for sciatic nerve regeneration study. Schematic overview of the fabrication process,[1,2] SEM morphology,[3–5] and stability of the printed constructs[6] used in the study. The NGF release profile[7] from the fabricated constructs at indicated time points. Reproduced under the terms of CC-BY license.[210] Copyright 2022, The Authors, published by Elsevier.

allel, packed, and ordered fibers and has a complicated structure. In skeletal-muscle regeneration, significant research is being done on designing and constructing porous scaffolds to engineer tissues to repair defects caused by traumas, tears, myopathies, ischemia, and injuries during the surgical procedure. These porous scaffolds, however, have inherent limitations, such as nonuniform and ill-controlled cell dispersion, cell in-growth, and restricted control of the scaffold microarchitecture.[213] Biomaterials such as hydrogels, fibrous meshes, and micropatterned substrates have been used to stimulate vascularization and innervation, induce contractility, and enhance myogenic alignment and fusion, resulting in myotubes for skeletal muscle regeneration.[214,215] For example, a bilayer scaffold made up of anisotropic methacrylated alginate (ALMA) fibers and aligned polycaprolactone (PCL) fibers were electrospun and then forced to self-fold in a calcium ion solution to generate multilayer scroll-like tubular constructions encasing myoblast cells. Because ALMA and PCL are inert and do not adhere to cells, scaffolds were coated with FNC solution (fibronectin, collagen, and albumin) to enhance cell attachment. This construct pro-

vided a milieu for myoblast cells to align, elongate, differentiate, and fuse to myotubes inside the self-rolled multilayer construct, resulting in native-like skeletal-muscle fibers. Furthermore, studies revealed that when mature myotubes arranged along fibers were electrically stimulated, they showed synchronized contractions.

In another study by Kim et al., using 3D bioprinting, decellularized ECM methacrylate (dECM-MA) from pig skeletal muscles was mixed with fibrillated poly(vinyl alcohol) (PVA) to form a uniaxially orientated patterned material.[216] The dECM-tissue-specific MA's biochemical cues were integrated with topographical cues. The C2C12 cell line's integrated myoblasts aligned, resulting in a high degree of myotube development. Furthermore, dECM composites contributed to higher expression of MyoD1, MYH2, and MyoG (myogenic genes), contrasted to GelMA composites with similar topographic signals. Choi et al. used a dECM bioink of skeletal muscle and a granule-based printing reservoir to generate structures such as dECM-based (sponges, hydrogels, and 3D cell-printed muscle constructs).[59] In a volumetric muscle loss (VML) rat model, the 3D-printed muscle constructions demonstrated increased viability of cells without generating an oxygen-deprived microenvironment, maintaining aligned and densely populated muscle fibers across the composite, and the de novo muscle development was found to be increased. Furthermore, prevascularized muscle constructions were created by employing vascular dECM as bioink and coaxial nozzle printing method, resulting in increased de novo muscle fiber production, innervation angiogenesis, and 85% improved function in the VML rat model. The extrusion pressure and proper choice of nozzle shape and size proved effective for cell orientation in 3D-printing technology.[217]

6.5. Application in Skin Tissue Engineering

The skin is the largest organ in the human body, and it regulates temperature, controls evaporation, and protects against viruses and the outside environment. The epidermis, the outer layer, is followed by the dermis, which is infiltrated by a complex nerve and blood artery network, and the hypodermis, which comprises subcutaneous tissue.[218] As a result, several researchers have attempted to replace this complicated and vital organ with artificial skin grafts such as hydrogels to treat skin wounds and disorders in skin tissue engineering.[219] Recent advancements in hydrogel printing techniques, which have gone from 2D to 3D printing, have allowed for increased micro/nanostructural management flexibility. Furthermore, research concentrates on 3D-printing hydrogel composites to functionalize hydrogel scaffolds that resemble genuine skin tissue.

Skardal et al. examined the feasibility of printed amniotic fluid-derived stem (AFS) cells incorporating hydrogels regenerating a mouse skin wound.[220] They made hydrogel composites with fibrinogen/collagen combined in a 50:50 volume ratio and hydrogel composites with AFS cells and mesenchymal stem cells (MSCs). Inkjet 3D printers were used to layer-by-layer print fibrinogen/collagen hydrogel composites with cells and thrombin on the skin wound of a nude mouse. Wounds treated with a composite containing AFS and MSC cells had better wound closure and re-epithelialization results after 14 days than wounds treated with a fibrin/collagen gel, with increased vascular density and larger capillary diameters.

For tissue engineering, chitosan and graphene are hydrogel composite materials.[221,222] Because of its HA concentration and glycosaminoglycans in joints, chitosan has been employed in artificial skin and wound dressing.[223] Chitosan or methacrylated chitosan (ChiMA) was combined with varying quantities of graphene and extruded by a customized computer numerical control machine in Sayyar's experiments. Both graphene/chitosan and graphene/ChiMA hydrogels exhibited tunable swelling properties and good biocompatibility, as evidenced by fibroblast proliferation and cell adhesion assays on the hydrogel constructs. Tensile strength and conductivity increased significantly as the amount of graphene in chitosan or ChiMA increased.

7. Concerns and Challenges of Photocurable 3D Printing

The bioink used in 3D printing is essential in providing a suitable microenvironment for native cells and tissues. Massive efforts should be made to examine the bioinks resembling tissue-specific ECM properties. The existing bioinks only imitate the composition of ECM without appropriate geometry, resulting in unsatisfactory outcomes.[224] Bioprinted tissue lacks angiogenesis, which is crucial for supplying oxygen and nutrients, and prolonged cell survival. Thus, the majority of the tissue construct depends upon the diffusion for nutrient supply and limits the functionality of printed structures.[225]

The viscosity and performance of the photocurable resins determine the quality of the final product. The high viscosity and molecular weight of the photocurable resin restrict printing performance. Low viscosity resins are of small molecular weight, which causes the material to attain a high degree of crosslinking. Therefore, it provides the material rigidity and brittleness. However, resins with low viscosity are imperative to develop to avoid the complications linked with the high viscosity.[226] Some photocurable polymers exhibit a low photoresistive effect and poor mechanical properties, limiting their uses in the bioprinting of complex structures.[227]

Photopolymers undergo curing upon exposure to light of a specific wavelength and form polymer networks. The partially cured polymer resin requires a post-curing step to cure and solidify the liquid resins. However, the post-curing for an extended period results in over-curing, affecting the object's final characteristics, including shrinkage and loss of accuracy.[18] The elastic property of the material is essential to consider to obtain an object with high elasticity. High viscosity photosensitive resins exhibit excellent elasticity and toughness. Therefore, printing high-viscosity resins with the available printing techniques is challenging. New printing techniques must be developed to print highly viscous resin.[226]

Printing the objects with high accuracy is vital to simulate the structure of native tissue. Pore size, shape, and resolution rely on printing techniques. The DLP printers build structures of small size, whereas the SLA prints large-sized structures with low efficiency, which is a significant concern in manufacturing large-size structures.[226] Most printers used for pharmaceutical formulation do not follow GMP regulations. Thus, validation is necessary

to ensure the final product satisfies the safety requirements.[228] For the successful printing of complex structures, parameters such as nozzle size, printer type, and the physicochemical properties of the materials should be considered.

The challenges mentioned above hurdle the application of photocurable 3D printing in tissue engineering applications; developing ongoing printing techniques to overcome these problems will help design the structures with high precision and accuracy.

8. Conclusion and Future Outlook

The advent and revolutionary development of 3D-printing technology have made it possible to fabricate complex equipment in various industries. We have highlighted and envisioned the growth of 3D-printing-based technology in several areas in this manuscript. The demand for organ substitutes in patients continues to rise due to a lack of donors and biocompatibility problems in transplant immunological rejection. Scientists have developed bioartificial organs that can be printed rather than implanted to address these concerns. Photopolymerization-based 3D-printing technologies such as SLA, DLP, and CLIP allow for the relatively rapid and controlled fabrication of various architectures without molds. 3D printing has opened new directions in different tissue engineering and regenerative medicine by utilizing polymer chemistry-related advancements. Despite its rapid expansion, it nevertheless confronts several hurdles that limit its potential to progress. Such as, new researches are needed to improve the characteristics of printed composites with functional features that can be reactivated to provide new qualities in a living manner. At present, additives such as photocatalysts are used for producing free radicals; the alteration and effects of photocatalysts on the properties of the designed material should be carefully evaluated. For environmental and health concerns, low-cost and naturally derived photocatalysts should be discovered. To avoid prolonged exposure during layer-by-layer deposition, fully automated 3D printers should be established for multilayered structures. The printing process releases volatile substances into the environment, which are detrimental to public health; therefore, the advancement of printers with low emission properties is needed. Moreover, hybrid manufacturing techniques, such as combining photopolymerization with the electrospinning method, will prove to be a progressive approach for producing complex structures that mimic the cell microenvironment. In conclusion, photopolymerization-based 3D printing has proven to be an effective technology in tissue engineering. In order to widen and increase the spectrum of applications, more innovative studies are required to modify the final quality of 3D-printed materials by enhancing the biocompatibility, designing with living features using controlled living radical polymerization techniques, tuneable physicochemical and mechanical properties, and evolving the 3D-printing methodology. The development of materials and new technologies to overcome the hurdles associated with the available techniques can prove to be a breakthrough in the 3D-printing field.

Supporting Information

Supporting Information is available from the Wiley Online Library or from the author.

Acknowledgements

A.R. and S.D.D. contributed equally to this work. This research was supported by Basic Research Program through the National Research Foundation of Korea (NRF), which is financed by the Ministry of Education (no. 2018R1A6A1A03025582, no. 2019R1D1A3A03103828, and no. 2022R1I1A3063302), Republic of Korea.

Conflict of Interest

The authors declare no conflict of interest.

Keywords

3D printing, biopolymers, photopolymerization, printability, tissue engineering

Received: July 6, 2022
Revised: September 9, 2022
Published online:

[1] A. M. Pekkanen, R. J. Mondschein, C. B. Williams, T. E. Long, *Biomacromolecules.* **2017**, *18*, 2669.
[2] M. Guvendiren, J. Molde, R. M. D. Soares, J. Kohn, *ACS Biomater. Sci. Eng.* **2016**, *2*, 1679.
[3] M. Layani, X. Wang, S. Magdassi, *Adv. Mater.* **2018**, *30*, 1706344.
[4] J. Zhang, P. Xiao, *Polym. Chem.* **2018**, *9*, 1530.
[5] B. Baroli, *J. Chem. Technol. Biotechnol.* **2006**, *81*, 491.
[6] S. Lu, *J. Controlled Release* **1999**, *57*, 291.
[7] R. D. Jones, H. B. Jampani, J. L. Newman, A. S. Lee, *Am. J. Infect. Control* **2000**, *28*, 184.
[8] R. G. Schoenmakers, P. Van De Wetering, D. L. Elbert, J. A. Hubbell, *J. Controlled Release* **2004**, *95*, 291.
[9] M. D. Goodner, C. N. Bowman, *Chem. Eng. Sci.* **2002**, *57*, 887.
[10] S. Yokoyama, T. Nakahama, H. Miki, S. Mashiko, *Thin Solid Films* **2003**, *438*, 452.
[11] K. Itoga, M. Yamato, J. Kobayashi, A. Kikuchi, T. Okano, *J. Biomed. Mater. Res., Part A* **2004**, *69*, 391.
[12] J. Fu, H. Yin, X. Yu, C. Xie, H. Jiang, Y. Jin, F. Sheng, *Int. J. Pharm.* **2018**, *549*, 370.
[13] A. Bagheri, J. Jin, *ACS Appl. Polym. Mater.* **2019**, *1*, 593.
[14] J. W. Stansbury, M. J. Idacavage, *Dent. Mater.* **2016**, *32*, 54.
[15] J. Zhang, F. Dumur, P. Xiao, B. Graff, D. Gigmes, J. Pierre Fouassier, J. Lalevée, *J. Polym. Sci., Part A: Polym. Chem.* **2016**, *54*, 1189.
[16] S. V. Murphy, A. Atala, *Nat. Biotechnol.* **2014**, *32*, 773.
[17] Q. Zhang, H-P Bei, M. Zhao, Z. Dong, X. Zhao, *Biomaterials* **2022**, *286*, 121566.
[18] G. Taormina, C. Sciancalepore, M. Messori, F. Bondioli, *J. Appl. Biomater. Funct. Mater.* **2018**, *16*, 151.
[19] B. Wendel, D. Rietzel, F. Kühnlein, R. Feulner, G. Hülder, E. Schmachtenberg, *Macromol. Mater. Eng.* **2008**, *293*, 799.
[20] M. Askari, D. A. Hutchins, P. J. Thomas, L. Astolfi, R. L. Watson, M. Abdi, M. Ricci, S. Laureti, L. Nie, S. Freear, R. Wildman, C. Tuck, M. Clarke, E. Woods, A. T. Clare, *Addit. Manuf.* **2020**, *36*, 101562.
[21] T. D. Ngo, A. Kashani, G. Imbalzano, K. T. Q. Nguyen, D. Hui, *Composites, Part B* **2018**, *143*, 172.
[22] Y. Yoo, H. Hyun, S.-J. Yoon, S. Y. Kim, D.-W. Lee, S. Um, S. O. Hong, D. H. Yang, *J. Ind. Eng. Chem.* **2018**, *67*, 365.
[23] T. Billiet, M. Vandenhaute, J. Schelfhout, S. Van Vlierberghe, P. Dubruel, *Biomaterials* **2012**, *33*, 6020.
[24] A. Farzan, S. Borandeh, N. Zanjanizadeh Ezazi, S. Lipponen, H. L. A. Santos, J. Seppälä, *Eur. Polym. J.* **2020**, *139*, 109988.

[25] B. Huang, R. Hu, Z. Xue, J. Zhao, Q. Li, T. Xia, W. Zhang, C. Lu, *Carbohydr. Polym.* **2020**, *231*, 115736.
[26] T. M. Seck, F. P. W. Melchels, J. Feijen, D. W. Grijpma, *J. Controlled Release* **2010**, *148*, 34.
[27] I. Shiraishi, M. Yamagishi, K. Hamaoka, M. Fukuzawa, T. Yagihara, *Eur. J. Cardio-Thoracic Surg.* **2010**, *37*, 302.
[28] K. Kowsari, B. Zhang, S. Panjwani, Z. Chen, H. Hingorani, S. Akbari, N. X. Fang, Q. Ge, *Addit. Manuf.* **2018**, *24*, 627.
[29] Y. Shao, Z. Liao, B. Gao, B. He, *ACS Omega* **2022**, *7*, 11530.
[30] J. Li, C. Boyer, X. Zhang, *Macromol. Mater. Eng.* **2022**, *307*, 2200010.
[31] T. P. Glenn, S. Webster, R. D. Hollaway, *US6624921* **2003**.
[32] R. Felzmann, S. Gruber, G. Mitteramskogler, P. Tesavibul, A. R. Boccaccini, R. Liska, J. Stampfl, *Adv. Eng. Mater.* **2012**, *14*, 1052.
[33] B. Zhang, R. Cristescu, D. B. Chrisey, R. J. Narayan, *Int. J. Bioprint.* **2020**, *6*, 19.
[34] M. Rajput, P. Mondal, P. Yadav, K. Chatterjee, *Int. J. Biol. Macromol.* **2022**, *202*, 644.
[35] D. Dean, J. Wallace, A. Siblani, M. O. Wang, K. Kim, A. G. Mikos, J. P. Fisher, *Virtual Phys. Prototyping.* **2012**, *7*, 13.
[36] K. S. Lim, R. Levato, P. F. Costa, M. D. Castilho, C. R. Alcala-Orozco, K. M. A. Van Dorenmalen, F. P. W. Melchels, D. Gawlitta, G. J. Hooper, J. Malda, T. B. F. Woodfield, *Biofabrication* **2018**, *10*, 034101.
[37] X. Kuang, J. Wu, K. Chen, Z. Zhao, Z. Ding, F. Hu, D. Fang, H. J. Qi, *Sci. Adv.* **2019**, *5*, eaav5790.
[38] H. Hong, Y. B. Seo, D. Y. Kim, J. S. Lee, Y. J. Lee, H. Lee, O. Ajiteru, M. T. Sultan, O. J. Lee, S. H. Kim, C. H. Park, *Biomaterials* **2020**, *232*, 119679.
[39] J. R. Tumbleston, D. Shirvanyants, N. Ermoshkin, R. Janusziewicz, A. R. Johnson, D. Kelly, K. Chen, R. Pinschmidt, J. P. Rolland, A. Ermoshkin, E. T. Samulski, J. M. Desimone, *Science* **2015**, *347*, 1349.
[40] R. Janusziewicz, J. R. Tumbleston, A. L. Quintanilla, S. J. Mecham, J. M. Desimone, *Proc. Natl. Acad. Sci. U. S. A.* **2016**, *113*, 11703.
[41] R. F. Pereira, P. J. Bártolo, *Engineering* **2015**, *1*, 090.
[42] B. D. Fairbanks, M. P. Schwartz, C. N. Bowman, K. S. Anseth, *Biomaterials* **2009**, *30*, 6702.
[43] H. Shih, C.-C. Lin, *Macromol. Rapid Commun.* **2013**, *34*, 269.
[44] S. C. Ligon, R. Liska, J. Stampfl, M. Gurr, R. Mülhaupt, *Chem. Rev.* **2017**, *117*, 10212.
[45] J. P. Fouassier, X. Allonas, J. Lalevée, C. Dietlin, in *Photochemistry and Photophysics of Polymer Materials* (Ed: N. S. Allen), Wiley, New York **2010**, pp. 351–419.
[46] F. Jasinski, P. B. Zetterlund, A. M. Braun, A. Chemtob, *Prog. Polym. Sci.* **2018**, *84*, 47.
[47] D. D. M. Wayner, K. B. Clark, A. Rauk, D. Yu, D. A. Armstrong, *J. Am. Chem. Soc.* **1997**, *119*, 8925.
[48] S. C. Ligon-Auer, M. Schwentenwein, C. Gorsche, J. Stampfl, R. Liska, *Polym. Chem.* **2016**, *7*, 257.
[49] C. E. Hoyle, T. Y. Lee, T. Roper, *J. Polym. Sci., Part A: Polym. Chem.* **2004**, *42*, 5301.
[50] B. Husár, S. C. Ligon, H. Wutzel, H. Hoffmann, R. Liska, *Prog. Org. Coat.* **2014**, *77*, 1789.
[51] C. E. Hoyle, C. N. Bowman, *Angew. Chem., Int. Ed.* **2010**, *49*, 1540.
[52] S. C. Ligon, B. Husár, H. Wutzel, R. Holman, R. Liska, *Chem. Rev.* **2014**, *114*, 557.
[53] A. Oesterreicher, J. Wiener, M. Roth, A. Moser, R. Gmeiner, M. Edler, G. Pinter, T. Griesser, *Polym. Chem.* **2016**, *7*, 5169.
[54] S. Bertlein, G. Brown, K. S. Lim, T. Jungst, T. Boeck, T. Blunk, J. Tessmar, G. J. Hooper, T. B. F. Woodfield, J. Groll, *Adv. Mater.* **2017**, *29*, 1703404.
[55] J. Kumpfmueller, K. Stadlmann, Z. Li, V. Satzinger, J. Stampfl, R. Liska, *Des. Monomers Polym.* **2014**, *17*, 390.
[56] A. S. Quick, J. Fischer, B. Richter, T. Pauloehrl, V. Trouillet, M. Wegener, C. Barner-Kowollik, *Macromol. Rapid Commun.* **2013**, *34*, 335.
[57] B. D. Fairbanks, E. A. Sims, K. S. Anseth, C. N. Bowman, *Macromolecules* **2010**, *43*, 4113.
[58] J. W. Chan, J. Shin, C. E. Hoyle, C. N. Bowman, A. B. Lowe, *Macromolecules* **2010**, *43*, 4937.
[59] Y.-J. Choi, Y.-J. Jun, D. Y. Kim, H.-G. Yi, S.-H. Chae, J. Kang, J. Lee, G. Gao, J.-S. Kong, J. Jang, W. K. Chung, J.-W. Rhie, D.-W. Cho, *Biomaterials* **2019**, *206*, 160.
[60] K. J. Schafer, J. M. Hales, M. Balu, K. D. Belfield, E. W. Van Stryland, D. J. Hagan, *J. Photochem. Photobiol., A* **2004**, *162*, 497.
[61] M. R. Melhem, J. Park, L. Knapp, L. Reinkensmeyer, C. Cvetkovic, J. Flewellyn, M. K. Lee, T. W. Jensen, R. Bashir, H. Kong, L. B. Schook, *ACS Biomater. Sci. Eng.* **2017**, *3*, 1980.
[62] R. Gauvin, Y.-C. Chen, J. W. Lee, P. Soman, P. Zorlutuna, J. W. Nichol, H. Bae, S. Chen, A. Khademhosseini, *Biomaterials* **2012**, *33*, 3824.
[63] B. K. Mann, A. S. Gobin, A. T. Tsai, R. H. Schmedlen, J. L. West, *Biomaterials* **2001**, *22*, 3045.
[64] A. Chiappone, E. Fantino, I. Roppolo, M. Lorusso, D. Manfredi, P. Fino, C. F. Pirri, F. Calignano, *ACS Appl. Mater. Interfaces* **2016**, *8*, 5627.
[65] E. Fantino, A. Chiappone, F. Calignano, M. Fontana, F. Pirri, I. Roppolo, *Materials* **2016**, *9*, 589.
[66] P. Occhetta, R. Visone, L. Russo, L. Cipolla, M. Moretti, M. Rasponi, *J. Biomed. Mater. Res., Part A* **2015**, *103*, 2109.
[67] J. Warner, P. Soman, W. Zhu, M. Tom, S. Chen, *ACS Biomater. Sci. Eng.* **2016**, *2*, 1763.
[68] D. Manojlovic, M. D. Dramiä‡Anin, M. Lezaja, P. Pongprueksa, B. Van Meerbeek, V. Miletic, *Dent. Mater.* **2016**, *32*, 183.
[69] H. K. Park, M. Shin, B. Kim, J. W. Park, H. Lee, *NPG Asia Mater.* **2018**, *10*, 82.
[70] N. B. Palaganas, J. D. Mangadlao, A. C. C. de Leon, J. O. Palaganas, K. D. Pangilinan, Y. J. Lee, R. C. Advincula, *ACS Appl. Mater. Interfaces* **2017**, *9*, 34314.
[71] B. P. Fors, C. J. Hawker, *Angew. Chem. Int. Ed. Engl.* **2012**, *51*, 8850.
[72] A. Bagheri, H. Arandiyan, N. N. M. Adnan, C. Boyer, M. Lim, *Macromolecules* **2017**, *50*, 7137.
[73] J. Zhang, F. Dumur, P. Xiao, B. Graff, D. Bardelang, D. Gigmes, J. P. Fouassier, J. Lalevée, *Macromolecules* **2015**, *48*, 2054.
[74] Z. Sadrearhami, J. Yeow, T.-K. Nguyen, K. K. K. Ho, N. Kumar, C. Boyer, *Chem. Commun.* **2017**, *53*, 12894.
[75] A. Bagheri, H. Arandiyan, C. Boyer, M. Lim, *Adv. Sci.* **2016**, *3*, 1500437.
[76] J. Wang, S. Stanic, A. A. Altun, M. Schwentenwein, K. Dietliker, L. Jin, J. Stampfl, S. Baudis, R. Liska, H. Grützmacher, *Chem. Commun.* **2018**, *54*, 920.
[77] S. Jauk, R. Liska, *J. Macromol. Sci., Part A: Pure Appl. Chem.* **2008**, *45*, 804.
[78] B. Ganster, U. K. Fischer, N. Moszner, R. Liska, *Macromolecules* **2008**, *41*, 2394.
[79] B. Steyrer, P. Neubauer, R. Liska, J. Stampfl, *Materials* **2017**, *10*, 1445.
[80] E. M. Chandler, C. M. Berglund, J. S. Lee, W. J. Polacheck, J. P. Gleghorn, B. J. Kirby, C. Fischbach, *Biotechnol. Bioeng.* **2011**, *108*, 1683.
[81] R. A. Dilla, C. M. M. Motta, S. R. Snyder, J. A. Wilson, C. Wesdemiotis, M. L. Becker, *ACS Macro Lett.* **2018**, *7*, 1254.
[82] J. Xu, K. Jung, C. Boyer, *Macromolecules* **2014**, *47*, 4217.
[83] J. Crivello, J. Lam, *J. Polym. Sci., Part A: Polym. Chem.* **1980**, *18*, 2677.
[84] Z. Huang, Y. Gu, X. Liu, L. Zhang, Z. Cheng, X. Zhu, *Macromol. Rapid Commun.* **2017**, *38*, 1600461.
[85] E. Zanchetta, M. Cattaldo, G. Franchin, M. Schwentenwein, J. Homa, G. Brusatin, P. Colombo, *Adv. Mater.* **2016**, *28*, 370.
[86] J. Yue, P. Zhao, J. Y. Gerasimov, M. Van De Lagemaat, A. Grotenhuis, M. Rustema-Abbing, H. C. Van Der Mei, H. J. Busscher, A. Herrmann, Y. Ren, *Adv. Funct. Mater.* **2015**, *25*, 6756.

[87] K. S. Lim, B. S. Schon, N. V. Mekhileri, G. C. Brown, C. M. Chia, S. Prabakar, G. J. Hooper, T. B. Woodfield, *ACS Biomater. Sci. Eng.* **2016**, *2*, 1752.
[88] X.-H. Qin, P. Gruber, M. Markovic, B. Plochberger, E. Klotzsch, J. Stampfl, A. Ovsianikov, R. Liska, *Polym. Chem.* **2014**, *5*, 6523.
[89] A. Al Mousawi, P. Garra, M. Schmitt, J. Toufaily, T. Hamieh, B. Graff, J. P. Fouassier, F. Dumur, J. Lalevée, *Macromolecules* **2018**, *51*, 4633.
[90] P. Xiao, F. Dumur, M. Frigoli, M.-A. Tehfe, B. Graff, J. P. Fouassier, D. Gigmes, J. Lalevée, *Polym. Chem.* **2013**, *4*, 5440.
[91] P. Xiao, F. Dumur, B. Graff, D. Gigmes, J. P. Fouassier, J. Lalevée, *Macromolecules* **2014**, *47*, 601.
[92] P. Xiao, F. Dumur, J. Zhang, J. P. Fouassier, D. Gigmes, J. Lalevée, *Macromolecules* **2014**, *47*, 3837.
[93] N. Corrigan, S. Shanmugam, J. Xu, C. Boyer, *Chem. Soc. Rev.* **2016**, *45*, 6165.
[94] B. P. Fors, C. J. Hawker, *Angew. Chem., Int. Ed.* **2012**, *51*, 8850.
[95] A. Ohtsuki, A. Goto, H. Kaji, *Macromolecules* **2013**, *46*, 96.
[96] P. V. Pham, D. A. Nagib, D. W. C. Macmillan, *Angew. Chem., Int. Ed.* **2011**, *50*, 6119.
[97] D. A. Nicewicz, D. W. C. Macmillan, *Science* **2008**, *322*, 77.
[98] S. Dadashi-Silab, S. Doran, Y. Yagci, *Chem. Rev.* **2016**, *116*, 10212.
[99] D. Konkolewicz, K. Schröder, J. Buback, S. Bernhard, K. Matyjaszewski, *ACS Macro Lett.* **2012**, *1*, 1219.
[100] M. R. Hill, R. N. Carmean, B. S. Sumerlin, *Macromolecules* **2015**, *48*, 5459.
[101] A. Al Mousawi, F. Dumur, P. Garra, J. Toufaily, T. Hamieh, B. Graff, D. Gigmes, J. P. Fouassier, J. Lalevée, *Macromolecules* **2017**, *50*, 2747.
[102] A. Schwab, R. Levato, M. D'Este, S. Piluso, D. Eglin, J. Malda, *Chem. Rev.* **2020**, *120*, 11028.
[103] A. Ribeiro, M. M. Blokzijl, R. Levato, C. W. Visser, M. Castilho, W. E. Hennink, T. Vermonden, J. Malda, *Biofabrication* **2017**, *10*, 014102.
[104] N. P. Cheremisinoff, *An Introduction to Polymer Rheology and Processing*, CRC Press, Boca Raton, FL **2018**.
[105] E. B. Montufar, Y. Maazouz, M. P. Ginebra, *Acta Biomater.* **2013**, *9*, 6188.
[106] J. M. G. Cowie, V. Arrighi. *Polymers: Chemistry and Physics of Modern Materials*, CRC Press, Boca Raton, FL **2007**.
[107] T. Mezger. *The Rheology Handbook*, 3rd ed., Vincentz Network Publication, Hanover **2011**.
[108] S. Kyle, Z. M. Jessop, A. Al-Sabah, I. S. Whitaker, *Adv. Healthcare Mater.* **2017**, *6*, 1700264.
[109] A. Randles, D. H. Frakes, J. A. Leopold, *Trends Biotechnol.* **2017**, *35*, 1049.
[110] A. Shafiee, M. Mccune, G. Forgacs, I. Kosztin, *Biofabrication* **2015**, *7*, 045005.
[111] C. J. Doillon, F. H. Silver, *Biomaterials* **1986**, *7*, 3.
[112] C. Wiegand, B. A. Buhren, E. Bünemann, H. Schrumpf, B. Homey, R. G. Frykberg, F. Lurie, P. A. Gerber, *J. Wound Care* **2016**, *25*, 713.
[113] S. T. Bendtsen, M. Wei, *J. Mater. Chem. B* **2015**, *3*, 3081.
[114] D. Wei, J. Sun, J. Bolderson, M. Zhong, M. J. Dalby, M. Cusack, H. Yin, H. Fan, X. Zhang, *ACS Appl. Mater. Interfaces* **2017**, *9*, 14606.
[115] H. Hyun, M. Park, G. Jo, S. Kim, H. Chun, D. Yang, *Marine Drugs* **2019**, *17*, 41.
[116] Y. Yoo, S.-J. Yoon, S. Y. Kim, D.-W. Lee, S. Um, H. Hyun, S. O. Hong, D. H. Yang, *Drug Delivery* **2018**, *25*, 1664.
[117] H. Hyun, M. H. Park, W. Lim, S. Y. Kim, D. Jo, J. S. Jung, G. Jo, S. Um, *Artif. Cells, Nanomed., Biotechnol.* **2018**, *46*, 874.
[118] F. J. O'Brien, *Mater. Today* **2011**, *14*, 88.
[119] O. Jeon, K. H. Bouhadir, J. M. Mansour, E. Alsberg, *Biomaterials* **2009**, *30*, 2724.
[120] A. I. Chou, S. B. Nicoll, *J. Biomed. Mater. Res., Part A* **2009**, *91A*, 187.
[121] D. S. Lima, E. T. Tenório-Neto, M. K. Lima-Tenório, M. R. Guilherme, D. B. B. Scariot, C. V. Nakamura, E. C. Muniz, A. F. Rubira, *J. Mol. Liq.* **2018**, *262*, 29.
[122] A. D. Rouillard, C. M. Berglund, J. Y. Lee, W. J. Polacheck, Y. Tsui, L. J. Bonassar, B. J. Kirby, *Tissue Eng., Part C* **2010**, *17*, 173.
[123] O. Jeon, C. Powell, L. D. Solorio, M. D. Krebs, E. Alsberg, *J. Controlled Release* **2011**, *154*, 258.
[124] N. K. Yaghi, J. Wei, Y. Hashimoto, L.-Y. Kong, K. Gabrusiewicz, E. K. Nduom, X. Ling, N. Huang, S. Zhou, B. C. Parker Kerrigan, J. M. Levine, V. R. Fajt, G. Levine, B. F. Porter, E. G. Marcusson, K. Tachikawa, P. Chivukula, D. C. Webb, J. E. Payne, A. B. Heimberger, *Neuro-Oncology* **2016**, *19*, 372.
[125] O. Jeon, E. Alsberg, *Tissue Eng., Part A* **2013**, *19*, 1424.
[126] N. K. Yaghi, J. Wei, Y. Hashimoto, L.-Y. Kong, K. Gabrusiewicz, E. K. Nduom, X. Ling, N. Huang, S. Zhou, B. C. P. Kerrigan, J. M. Levine, V. R. Fajt, G. Levine, B. F. Porter, E. G. Marcusson, K. Tachikawa, P. Chivukula, D. C. Webb, J. E. Payne, A. B. Heimberger, *Neuro-Oncology* **2016**, *19*, 372.
[127] O. Jeon, C. Powell, S. M. Ahmed, E. Alsberg, *Tissue Eng., Part A* **2010**, *16*, 2915.
[128] O. Jeon, D. W. Wolfson, E. Alsberg, *Adv. Mater.* **2015**, *27*, 2216.
[129] J. Sun, W. Xiao, Y. Tang, K. Li, H. Fan, *Soft Matter* **2012**, *8*, 2398.
[130] A. K. Kundu, A. J. Putnam, *Biochem. Biophys. Res. Commun.* **2006**, *347*, 347.
[131] M. Hasany, S. Talebian, S. Sadat, N. Ranjbar, M. Mehrali, G. G. Wallace, M. Mehrali, *Appl. Mater. Today* **2021**, *24*, 101150.
[132] J. A. Burdick, G. D. Prestwich, *Adv. Mater.* **2011**, *23*, H41.
[133] Y. Lei, S. Gojgini, J. Lam, T. Segura, *Biomaterials* **2011**, *32*, 39.
[134] L. Bian, M. Guvendiren, R. L. Mauck, J. A. Burdick, *Proc. Natl. Acad. Sci. U. S. A.* **2013**, *110*, 10117.
[135] B. Tavsanli, O. Okay, *Eur. Polym. J.* **2017**, *94*, 185.
[136] S. Sahoo, C. Chung, S. Khetan, J. A. Burdick, *Biomacromolecules* **2008**, *9*, 1088.
[137] Y. Ding, Z. Song, Q. Liu, S. Wei, L. Zhou, J. Zhou, J. Shen, *Dalton Trans.* **2017**, *46*, 11875.
[138] H. Chang, M. Zheng, X. Yu, A. Than, R. Z. Seeni, R. Kang, J. Tian, D. P. Khanh, L. Liu, P. Chen, C. Xu, *Adv. Mater.* **2017**, *29*, 1702243.
[139] K. Gwon, E. Kim, G. Tae, *Acta Biomater.* **2017**, *49*, 284.
[140] T. J. Whitehead, C. O. C. Avila, H. G. Sundararaghavan, *J. Biomed. Mater. Res., Part A* **2018**, *106*, 17.
[141] M. T. Poldervaart, B. Goversen, M. De Ruijter, A. Abbadessa, F. P. W. Melchels, F. Cumhur Öner, W. J. A. Dhert, T. Vermonden, J. Alblas, *PLoS One* **2017**, *12*, e0177628.
[142] B. Duan, Z. Yin, L. Hockaday Kang, R. L. Magin, J. T. Butcher, *Acta Biomater.* **2016**, *36*, 42.
[143] J. W. S. Hayami, S. D. Waldman, B. G. Amsden, *Macromol. Biosci.* **2016**, *16*, 1083.
[144] P. Khoshakhlagh, M. J. Moore, *Acta Biomater.* **2015**, *16*, 23.
[145] E. C. Beck, M. Barragan, T. B. Libeer, S. L. Kieweg, G. L. Converse, R. A. Hopkins, C. J. Berkland, M. S. Detamore, *Tissue Eng., Part A* **2016**, *22*, 665.
[146] J. R. Choi, K. W. Yong, J. Y. Choi, A. C. Cowie, *BioTechniques* **2019**, *66*, 40.
[147] B. Duan, E. Kapetanovic, L. A. Hockaday, J. T. Butcher, *Acta Biomater.* **2014**, *10*, 1836.
[148] B. J. Klotz, D. Gawlitta, A. J. W. P. Rosenberg, J. Malda, F. P. W. Melchels, *Trends Biotechnol.* **2016**, *34*, 394.
[149] J.-Y. Lai, Y.-T. Li, *Biomacromolecules* **2010**, *11*, 1387.
[150] K. Yue, G. Trujillo-De Santiago, M. M. Alvarez, A. Tamayol, N. Annabi, A. Khademhosseini, *Biomaterials* **2015**, *73*, 254.
[151] Y. Liu, M. B. Chan-Park, *Biomaterials* **2010**, *31*, 1158.
[152] A. I. Van Den Bulcke, B. Bogdanov, N. De Rooze, E. H. Schacht, M. Cornelissen, H. Berghmans, *Biomacromolecules* **2000**, *1*, 31.
[153] Y.-C. Chen, R.-Z. Lin, H. Qi, Y. Yang, H. Bae, J. M. Melero-Martin, A. Khademhosseini, *Adv. Funct. Mater.* **2012**, *22*, 2027.
[154] A. H. Nguyen, J. Mckinney, T. Miller, T. Bongiorno, T. C. Mcdevitt, *Acta Biomater.* **2015**, *13*, 101.

[155] J. Zhou, D. Yao, Z. Qian, S. Hou, L. Li, A. T. A. Jenkins, Y. Fan, *Biomaterials* **2018**, *161*, 11.
[156] P. Song, M. Li, B. Zhang, X. Gui, Y. Han, L. Wang, W. Zhou, L. Guo, Z. Zhang, Z. Li, C. Zhou, Y. Fan, X. Zhang, *Composites, Part B* **2022**, *244*, 110163.
[157] R. Levato, W. R. Webb, I. A. Otto, A. Mensinga, Y. Zhang, M. Van Rijen, R. Van Weeren, I. M. Khan, J. Malda, *Acta Biomater.* **2017**, *61*, 41.
[158] A. H. Sadeghi, S. R. Shin, J. C. Deddens, G. Fratta, S. Mandla, I. K. Yazdi, G. Prakash, S. Antona, D. Demarchi, M. P. Buijsrogge, J. P. G. Sluijter, J. Hjortnaes, A. Khademhosseini, *Adv. Healthcare Mater.* **2017**, *6*, 1601434.
[159] Y. S. Zhang, F. Davoudi, P. Walch, A. Manbachi, X. Luo, V. Dell'erba, A. K. Miri, H. Albadawi, A. Arneri, X. Li, X. Wang, M. R. Dokmeci, A. Khademhosseini, R. Oklu, *Lab Chip* **2016**, *16*, 4097.
[160] L. Fan, C. Liu, X. Chen, Y. Zou, Z. Zhou, C. Lin, G. Tan, L. Zhou, C. Ning, Q. Wang, *ACS Appl. Mater. Interfaces* **2018**, *10*, 17742.
[161] B. Byambaa, N. Annabi, K. Yue, G. Trujillo-De Santiago, M. M. Alvarez, W. Jia, M. Kazemzadeh-Narbat, S. R. Shin, A. Tamayol, A. Khademhosseini, *Adv. Healthcare Mater.* **2017**, *6*, 1700015.
[162] W. Jia, P. S. Gungor-Ozkerim, Y. S. Zhang, K. Yue, K. Zhu, W. Liu, Q. Pi, B. Byambaa, M. R. Dokmeci, S. R. Shin, A. Khademhosseini, *Biomaterials* **2016**, *106*, 58.
[163] S. P. Strand, K. Tømmeraas, K. M. Vårum, K. Østgaard, *Biomacromolecules* **2001**, *2*, 1310.
[164] T. Kean, M. Thanou, *Adv. Drug Delivery Rev.* **2010**, *62*, 3.
[165] D. F. Duarte Campos, W. Drescher, B. Rath, M. Tingart, H. Fischer, *CARTILAGE* **2012**, *3*, 205.
[166] M. N. V. R. Kumar, R. A. A. Muzzarelli, C. Muzzarelli, H. Sashiwa, A. J. Domb, *Chem. Rev.* **2004**, *104*, 6017.
[167] O. Felt, *Int. J. Pharm.* **1999**, *180*, 185.
[168] S. Patashnk, L. Rabinovich, G. Golomb, *J. Drug Targeting* **1997**, *4*, 371.
[169] E. Khor, L. Y. Lim, *Biomaterials* **2003**, *24*, 2339.
[170] M. C. Bonferoni, G. Sandri, S. Rossi, F. Ferrari, C. Caramella, *Expert Opin. Drug Delivery* **2009**, *6*, 923.
[171] N. D. Leipzig, R. G. Wylie, H. Kim, M. S. Shoichet, *Biomaterials* **2011**, *32*, 57.
[172] H. Sano, T. Yoshikawa, P. N. R. Pereira, N. Kanemura, M. Morigamui, J. Tagami, D. H. Pashley, *J. Dent. Res.* **1999**, *78*, 906.
[173] M. Diolosà, I. Donati, G. Turco, M. Cadenaro, R. Di Lenarda, L. Breschi, S. Paoletti, *Biomacromolecules* **2014**, *15*, 4606.
[174] D. G. O'Shea, C. M. Curtin, F. J. O'Brien, *Biomater. Sci.* **2022**, *10*, 2462.
[175] K. E. Drzewiecki, A. S. Parmar, I. D. Gaudet, J. R. Branch, D. H. Pike, V. Nanda, D. I. Shreiber, *Langmuir* **2014**, *30*, 11204.
[176] Z. Wu, J. Liu, J. Lin, L. Lu, J. Tian, L. Li, C. Zhou, *Biomacromolecules* **2021**, *23*, 240.
[177] Y. Xu, X. Jiang, C. Niu, S. Yang, X. Xiao, Z. Huang, L. Feng, *Macromol. Mater. Eng.* **2022**, *307*, 2100862.
[178] T. Jain, H. B. Baker, A. Gipsov, J. P. Fisher, A. Joy, D. S. Kaplan, I. Isayeva, *Bioprinting* **2021**, *22*, e00131.
[179] W. Liu, W. Bi, Y. Sun, L. Wang, X. Yu, R. Cheng, Y. Yu, W. Cui, *Mater. Sci. Eng., C* **2020**, *110*, 110670.
[180] Y. Piao, H. You, T. Xu, H.-P. Bei, I. Z. Piwko, Y. Y. Kwan, X. Zhao, *Eng. Regener.* **2021**, *2*, 47.
[181] C. Liu, T. Dai, X. Wu, J. Ma, J. Liu, S. Wu, L. Yang, H. Zhao, *J. Mater. Sci. Technol.* **2022**.
[182] Y. Cao, P. Cheng, S. Sang, C. Xiang, Y. An, X. Wei, Z. Shen, Y. Zhang, P. Li, *Regener. Biomater.* **2021**, *8*, rbab019.
[183] E. Tsanaktsidou, O. Kammona, C. Kiparissides, *Eur. Polym. J.* **2019**, *114*, 47.
[184] L. Ouyang, C. B. Highley, C. B. Rodell, W. Sun, J. A. Burdick, *ACS Biomater. Sci. Eng.* **2016**, *2*, 1743.
[185] V. H. M. Mouser, A. Abbadessa, R. Levato, W. E. Hennink, T. Vermonden, D. Gawlitta, J. Malda, *Biofabrication* **2017**, *9*, 015026.
[186] A. R. Osi, H. Zhang, J. Chen, Y. Zhou, R. Wang, J. Fu, et al., *ACS Appl. Mater. Interfaces* **2021**, *13*, 22902.
[187] N. Cankaya, *J. Chem. Soc. Pak.* **2019**, *41*, 240.
[188] H. K. Chang, D. H. Yang, M. Y. Ha, H. J. Kim, C. H. Kim, S. H. Kim, J. W. Choi, H. J. Chun, *Carbohydr. Polym.* **2022**, *287*, 119328.
[189] J. H. Teoh, A. Mozhi, V. Sunil, S. M. Tay, J. Fuh, C. H. Wang, *Adv. Funct. Mater.* **2021**, *31*, 2105932.
[190] S. Saxena, A. R. Ray, A. Kapil, G. Pavon-Djavid, D. Letourneur, B. Gupta, A. Meddahi-Pellé, *Macromol. Biosci.* **2011**, *11*, 373.
[191] P. Iyer, K. J. Walker, S. V. Madihally, *Biotechnol. Bioeng.* **2012**, *109*, 1314.
[192] Y. Shigemasa, K. Saito, H. Sashiwa, H. Saimoto, *Int. J. Biol. Macromol.* **1994**, *16*, 43.
[193] C.-J. Wu, A. K. Gaharwar, P. J. Schexnailder, G. Schmidt, *Materials* **2010**, *3*, 2986.
[194] P. Bordes, E. Pollet, L. Averous, *Prog. Polym. Sci.* **2009**, *34*, 125.
[195] J. R. Xavier, T. Thakur, P. Desai, M. K. Jaiswal, N. Sears, E. Cosgriff-Hernandez, R. Kaunas, A. K. Gaharwar, *ACS Nano* **2015**, *9*, 3109.
[196] A. K. Gaharwar, S. M. Mihaila, A. Swami, A. Patel, S. Sant, R. L. Reis, A. P. Marques, M. E. Gomes, A. Khademhosseini, *Adv. Mater.* **2013**, *25*, 3329.
[197] Z. Li, S. Li, J. Yang, Y. Ha, Q. Zhang, X. Zhou, C. He, *Carbohydr. Polym.* **2022**, *290*, 119469.
[198] B. Sanz, A. Albillos Sanchez, B. Tangey, K. Gilmore, Z. Yue, X. Liu, G. Wallace, *Biomedicines* **2020**, *9*, 16.
[199] D. Van Der Valk, C. Van Der Ven, M. Blaser, J. Grolman, P.-J. Wu, O. Fenton, L. Lee, M. Tibbitt, J. Andresen, J. Wen, A. Ha, F. Buffolo, A. Van Mil, C. Bouten, S. Body, D. Mooney, J. Sluijter, M. Aikawa, J. Hjortnaes, R. Langer, E. Aikawa, *Nanomaterials* **2018**, *8*, 296.
[200] E. Aikawa, P. Libby, *Circulation* **2017**, *135*, 1951.
[201] R. Gaetani, P. A. Doevendans, C. H. G. Metz, J. Alblas, E. Messina, A. Giacomello, J. P. G. Sluijter, *Biomaterials.* **2012**, *33*, 1782.
[202] R. Gaetani, D. A. M. Feyen, V. Verhage, R. Slaats, E. Messina, K. L. Christman, A. Giacomello, P. A. F. M. Doevendans, J. P. G. Sluijter, *Biomaterials* **2015**, *61*, 339.
[203] C. Ngan, A. Quigley, C. O'Connell, M. Kita, J. Bourke, G. G. Wallace, P. Choong, R. M. Kapsa, *3D Bioprinting*, (Ed. J. Crook), Springer, New York **2020**, pp. 229–242.
[204] C. M. A. P. Schuh, A. G. E. Day, H. Redl, J. Phillips, *Tissue Eng., Part A* **2018**, *24*, 1332.
[205] Y.-B. Lee, S. Polio, W. Lee, G. Dai, L. Menon, R. S. Carroll, S.-S. Yoo, *Exp. Neurol.* **2010**, *223*, 645.
[206] C. M. Owens, F. Marga, G. Forgacs, C. M. Heesch, *Biofabrication* **2013**, *5*, 045007.
[207] T. Bedir, S. Ulag, C. B. Ustundag, O. Gunduz, *Mater. Sci. Eng., C* **2020**, *110*, 110741.
[208] W. Zhu, J. K. George, V. J. Sorger, L. Grace Zhang, *Biofabrication* **2017**, *9*, 025002.
[209] J. Tao, H. Liu, W. Wu, J. Zhang, S. Liu, J. Zhang, Y. Huang, X. Xu, H. He, S. Yang, M. Gou, *Adv. Funct. Mater.* **2020**, *30*, 2004272.
[210] H. S. Lee, E. Y. Jeon, J. J. Nam, J. H. Park, I. C. Choi, S. H. Kim, J. J. Chung, K. Lee, J. W. Park, Y. Jung, *Acta Biomater.* **2022**, *141*, 219.
[211] J. Hartmann, F. B. Thalheimer, F. Höpfner, T. Kerzel, K. Khodosevich, D. García-González, H. Monyer, I. Diester, H. Buning, J. E. Carette, P. Fries, C. J. Buchholz, *Mol. Ther.–Methods Clin. Dev.* **2019**, *14*, 252.
[212] L. Rao, Y. Qian, A. Khodabukus, T. Ribar, N. Bursac, *Nat. Commun.* **2018**, *9*, 126.
[213] T. K. Merceron, M. Burt, Y.-J. Seol, H.-W. Kang, S. J. Lee, J. J. Yoo, A. Atala, *Biofabrication* **2015**, *7*, 035003.

[214] T. H. Qazi, D. J. Mooney, M. Pumberger, S. Geissler, G. N. Duda, *Biomaterials* **2015**, *53*, 502.
[215] G. Constante, I. Apsite, H. Alkhamis, M. Dulle, M. Schwarzer, A. Caspari, A. Synytska, S. Salehi, L. Lonov, *ACS Appl. Mater. Interfaces* **2021**, *13*, 12767.
[216] W. Kim, H. Lee, J. Lee, A. Atala, J. J. Yoo, S. J. Lee, G. H. Kim, *Biomaterials* **2020**, *230*, 119632.
[217] T. Distler, A. A. Solisito, D. Schneidereit, O. Friedrich, R. Detsch, A. R. Boccaccini, *Biofabrication* **2020**, *12*, 045005.
[218] H. Sugihara, S. Toda, S. Miyabara, Y. Kusaba, Y. Minami, *In Vitro Cell. Dev. Biol.: Anim.* **1991**, *27*, 142.
[219] D.-M. WA, *Wound Repair Regener.* **2004**, *12*, 591.
[220] A. Skardal, D. Mack, E. Kapetanovic, A. Atala, J. D. Jackson, J. Yoo, S. Soker, *Stem Cells Transl. Med.* **2012**, *1*, 792.
[221] S. Sayyar, S. Gambhir, J. Chung, D. L. Officer, G. G. Wallace, *Nanoscale* **2017**, *9*, 2038.
[222] S. Sayyar, E. Murray, B. C. Thompson, J. Chung, D. L. Officer, S. Gambhir, G. M. Spinks, G. G. Wallace, *J. Mater. Chem. B* **2015**, *3*, 481.
[223] J.-K. F. Suh, H. W. Matthew, *Biomaterials* **2000**, *21*, 2589.
[224] S. Wang, S. Zhao, J. Yu, Z. Gu, Y. Zhang, *Small* **2022**, *18*, 2201869.
[225] S. V. Murphy, P. De Coppi, A. Atala, *Nat. Biomed. Eng.* **2020**, *4*, 370.
[226] H. Quan, T. Zhang, H. Xu, S. Luo, J. Nie, X. Zhu, *Bioact. Mater.* **2020**, *5*, 110.
[227] C. Mendes-Felipe, J. Oliveira, I. Etxebarria, J. Vilas-Vilela, S. Lanceros-Mendez, *Adv. Mater. Technol.* **2019**, *4*, 1800618.
[228] S. Mohapatra, R. K. Kar, P. K. Biswal, S. Bindhani, *Sens. Int.* **2022**, *3*, 100146.

Aayushi Randhawa is a doctoral student of Biosystem Engineering at Kangwon National University, South Korea. She received her master's degree from Bangalore University, India. Her research interest is the synthesis of 3D printed structures for the healing and regeneration of damaged tissues.

Sayan Deb Dutta is a doctoral student of Biosystems Engineering at Kangwon National University, South Korea. He received his master's degree from the University of Kalyani, India. His research interest is the synthesis of multifunctional nanomaterials for 3D printing and nanotheranostic applications for tissue engineering.

Keya Ganguly is a doctoral student of Biosystems Engineering at Kangwon National University, South Korea. She received her master's degree from Presidency University, India. Her research interest is developing a nanoengineered scaffolding platform for smart biosensing and tissue engineering.

Dinesh K. Patel is a postdoctoral research fellow at the Institute of Forest Sciences, Kangwon National University, South Korea. He received his doctoral degree in Material Science and Engineering from the Indian Institute of Technology, Banaras, India. His research interest is the synthesis of biomimetic nanomaterials and their application in tissue engineering.

Tejal V. Patil is a doctoral student of Biosystems Engineering at Kangwon National University, South Korea. She received her master's degree from the Institute of Chemical Technology, Mumbai, India. Her research interest is the development of biomaterials and tissue engineering.

Ki-Taek Lim is a professor of Biosystems Engineering at Kangwon National University, South Korea. He received his doctoral degree from Seoul National University, South Korea, and joined as a postdoctoral research fellow at the University of Arkansas, USA. He has a strong knowledge of mechatronics and regenerative medicines. His research mainly focuses on developing the bio-nanorobotic system with novel bioreactors and stem cell cultures for tissue-engineering applications.